

# $\mathcal{PT}$ -Symmetric Quantum Mechanics

Carl M. Bender<sup>1</sup>, Stefan Boettcher<sup>2,3</sup>, and Peter N. Meisinger<sup>1</sup>

<sup>1</sup>*Department of Physics, Washington University, St. Louis, MO 63130, USA*

<sup>2</sup>*Center for Nonlinear Studies, Los Alamos National Laboratory, Los Alamos, NM 87545, USA*

<sup>3</sup>*CTSPS, Clark Atlanta University, Atlanta, GA 30314, USA*

(February 1, 2008)

This paper proposes to broaden the canonical formulation of quantum mechanics. Ordinarily, one imposes the condition  $H^\dagger = H$  on the Hamiltonian, where  $\dagger$  represents the mathematical operation of complex conjugation and matrix transposition. This conventional Hermiticity condition is sufficient to ensure that the Hamiltonian  $H$  has a real spectrum. However, replacing this mathematical condition by the weaker and more physical requirement  $H^\ddagger = H$ , where  $\ddagger$  represents combined parity reflection and time reversal  $\mathcal{PT}$ , one obtains new classes of complex Hamiltonians whose spectra are still real and positive. This generalization of Hermiticity is investigated using a complex deformation  $H = p^2 + x^2(ix)^\epsilon$  of the harmonic oscillator Hamiltonian, where  $\epsilon$  is a real parameter. The system exhibits two phases: When  $\epsilon \geq 0$ , the energy spectrum of  $H$  is real and positive as a consequence of  $\mathcal{PT}$  symmetry. However, when  $-1 < \epsilon < 0$ , the spectrum contains an infinite number of complex eigenvalues and a finite number of real, positive eigenvalues because  $\mathcal{PT}$  symmetry is spontaneously broken. The phase transition that occurs at  $\epsilon = 0$  manifests itself in both the quantum-mechanical system and the underlying classical system. Similar qualitative features are exhibited by complex deformations of other standard real Hamiltonians  $H = p^2 + x^{2N}(ix)^\epsilon$  with  $N$  integer and  $\epsilon > -N$ ; each of these complex Hamiltonians exhibits a phase transition at  $\epsilon = 0$ . These  $\mathcal{PT}$ -symmetric theories may be viewed as analytic continuations of conventional theories from real to complex phase space.

PACS number(s): 03.65-w, 03.65.Ge, 11.30.Er, 02.60.Lj

## I. INTRODUCTION

In a recent letter [1] a class of complex quantum-mechanical Hamiltonians of the form

$$H = p^2 + x^2(ix)^\epsilon \quad (\epsilon \text{ real}) \quad (1.1)$$

was investigated. Despite the lack of conventional Hermiticity the spectrum of  $H$  is real and positive for all  $\epsilon \geq 0$ . As shown in Fig. 11 and Fig. 1 of Ref. [1], the spectrum is discrete and each of the energy levels increases as a function of increasing  $\epsilon$ . We will argue below that the reality of the spectrum is a consequence of  $\mathcal{PT}$  invariance.

The operator  $\mathcal{P}$  represents parity reflection and the operator  $\mathcal{T}$  represents time reversal. These operators are defined by their action on the position and momentum operators  $x$  and  $p$ :

$$\begin{aligned} \mathcal{P} : x &\rightarrow -x, & p &\rightarrow -p, \\ \mathcal{T} : x &\rightarrow x, & p &\rightarrow -p, & i &\rightarrow -i. \end{aligned} \quad (1.2)$$

When the operators  $x$  and  $p$  are real, the canonical commutation relation  $[x, p] = i$  is invariant under both parity reflection and time reversal. We emphasize that this commutation relation remains invariant under  $\mathcal{P}$  and  $\mathcal{T}$  even if  $x$  and  $p$  are complex provided that the above transformations hold. In terms of the real and imaginary parts of  $x$  and  $p$ ,  $x = \text{Re } x + i \text{Im } x$  and  $p = \text{Re } p + i \text{Im } p$ , we have

$$\begin{aligned} \mathcal{P} : \text{Re } x &\rightarrow -\text{Re } x, & \text{Im } x &\rightarrow -\text{Im } x, \\ & \text{Re } p &\rightarrow -\text{Re } p, & \text{Im } p &\rightarrow -\text{Im } p, \\ \mathcal{T} : \text{Re } x &\rightarrow \text{Re } x, & \text{Im } x &\rightarrow -\text{Im } x, \\ & \text{Re } p &\rightarrow -\text{Re } p, & \text{Im } p &\rightarrow \text{Im } p. \end{aligned} \quad (1.3)$$

While there is as yet no proof that the spectrum of  $H$  in Eq. (1.1) is real [2], we can gain some insight regarding the reality of the spectrum of a  $\mathcal{PT}$ -invariant Hamiltonian  $H$  as follows: Note that eigenvalues of the operator  $\mathcal{PT}$  have the form  $e^{i\theta}$ . To see this, let  $\Psi$  be an eigenfunction of  $\mathcal{PT}$  with eigenvalue  $\lambda$ :  $\mathcal{PT}\Psi = \lambda\Psi$ . Recalling that  $(\mathcal{PT})^2 = 1$ , we multiply this eigenvalue equation by  $\mathcal{PT}$  and obtain  $\lambda^*\lambda = 1$ , where we have used the fact that  $i \rightarrow -i$  under  $\mathcal{PT}$ . Thus,  $\lambda = e^{i\theta}$ . We know that if two linear operators commute, they can be simultaneously diagonalized. By assumption, the operator  $\mathcal{PT}$  commutes with  $H$ . Of course, the situation here is complicated by the nonlinearity of the  $\mathcal{PT}$  operator ( $\mathcal{T}$  involves complex conjugation). However, let us suppose for now that the eigenfunctions  $\psi$  of  $H$  are simultaneously eigenfunctions of the operator  $\mathcal{PT}$  with eigenvalue  $e^{i\theta}$ . Then applying  $\mathcal{PT}$  to the eigenvalue equation  $H\psi = E\psi$ , we find that the energy  $E$  is real:  $E = E^*$ .

We have numerically verified the supposition that the eigenfunctions of  $H$  in Eq. (1.1) are also eigenfunctions of the operator  $\mathcal{PT}$  when  $\epsilon \geq 0$ . However, when  $\epsilon < 0$ , the  $\mathcal{PT}$  symmetry of the Hamiltonian is spontaneously broken; even though  $\mathcal{PT}$  commutes with  $H$ , the eigenfunctions of  $H$  are *not* all simultaneously eigenfunctions of  $\mathcal{PT}$ . For these eigenfunctions of  $H$  the energies are

complex. Thus, a transition occurs at  $\epsilon = 0$ . As  $\epsilon$  goes below 0, the eigenvalues as functions of  $\epsilon$  pair off and become complex, starting with the highest-energy eigenvalues. As  $\epsilon$  decreases, there are fewer and fewer real eigenvalues and below approximately  $\epsilon = -0.57793$  only one real energy remains. This energy then begins to increase with decreasing  $\epsilon$  and becomes infinite as  $\epsilon$  approaches  $-1$ . In summary, the theory defined by Eq. (1.1) exhibits two phases, an unbroken-symmetry phase with a purely real energy spectrum when  $\epsilon \geq 0$  and a spontaneously-broken-symmetry phase with a partly real and partly complex spectrum when  $\epsilon < 0$ .

A primary objective of this paper is to analyze the phase transition at  $\epsilon = 0$ . We will demonstrate that this transition occurs in the classical as well as in the quantum theory. As a classical theory, the Hamiltonian  $H$  describes a particle subject to complex forces, and therefore the trajectory of the particle lies in the complex- $x$  plane. The position and momentum coordinates of the particle are complex functions of  $t$ , a real time parameter. We are interested only in solutions to the classical equations of motion for which the energy of the particle is real. We will see that in the  $\mathcal{PT}$ -symmetric phase of the theory, the classical motion is periodic and is thus a complex generalization of a pendulum. We actually observe two kinds of closed classical orbits, one in which the particle oscillates between two complex turning points and another in which the particle follows a closed orbit. In many cases these closed orbits lie on an elaborate multisheeted Riemann surface. On such Riemann surfaces the closed periodic orbits exhibit remarkable knot-like topological structures. All of these orbits exhibit  $\mathcal{PT}$  symmetry; they are left-right symmetric with respect to reflections about the imaginary- $x$  axis in accordance with Eq. (1.3). In the broken-symmetry phase classical trajectories are no longer closed. Instead, the classical path spirals out to infinity. These spirals lack  $\mathcal{PT}$  symmetry.

There have been many previous instances of non-Hermitian  $\mathcal{PT}$ -invariant Hamiltonians in physics. Energies of solitons on a *complex* Toda lattice have been found to be real [3]. Hamiltonians rendered non-Hermitian by an imaginary external field have been used to study population biology [4] and to study delocalization transitions such as vortex flux-line depinning in type-II superconductors [5]. In these cases, initially real eigenvalues bifurcate into the complex plane due to the increasing external field, indicating the growth of populations or the unbinding of vortices.

The  $\mathcal{PT}$ -symmetric Hamiltonian considered in this paper has many generalizations: (i) Introducing a mass term of the form  $m^2 x^2$  yields a theory that exhibits several phase transitions; transitions occur at  $\epsilon = -1$  and  $\epsilon = -2$  as well as at  $\epsilon = 0$  [1]. (ii) Replacing the condition of Hermiticity by the weaker constraint of  $\mathcal{PT}$ -symmetry also allows one to construct new classes of quasi-exactly solvable quantum theories [6]. (iii) In this paper we con-

sider complex deformations of real Hamiltonians other than the harmonic oscillator. We show that Hamiltonians of the form

$$H = p^2 + x^{2K}(ix)^\epsilon \quad (1.4)$$

have the same qualitative properties as  $H$  in Eq. (1.1). As  $\epsilon$  decreases below 0, all of these theories exhibit a phase transition from an unbroken  $\mathcal{PT}$ -symmetric regime to a regime in which  $\mathcal{PT}$  symmetry is spontaneously broken.

The Hamiltonian  $H$  in (1.1) is especially interesting because it can be generalized to quantum field theory. A number of such generalizations have recently been examined. The  $\mathcal{PT}$ -symmetric scalar field theory described by the Lagrangian [7]

$$\mathcal{L} = \frac{1}{2}(\partial\phi)^2 + \frac{1}{2}m^2\phi^2 + g\phi^2(i\phi)^\epsilon \quad (\epsilon \geq 0) \quad (1.5)$$

is intriguing because it is not invariant under parity reflection. This is manifested by a nonzero value of  $\langle\phi\rangle$ . It is interesting that this broken symmetry persists even when  $\epsilon > 0$  is an even integer [7]. The Hamiltonian for this theory is not Hermitian and, therefore, the theory is not unitary in the conventional sense. However, there is strong evidence that the spectrum for this theory is real and bounded below. For  $\epsilon = 1$  one can understand the positivity of the spectrum in terms of summability. The weak-coupling expansion for a conventional  $g\phi^3$  theory is real, and apart from a possible overall factor of  $g$ , the Green's functions are formal power series in  $g^2$ . These series are not Borel summable because they do not alternate in sign. Nonsummability reflects the fact that the spectrum of the underlying theory is not bounded below. However, when we replace  $g$  by  $ig$ , the perturbation series remains real but now alternates in sign. Thus, the perturbation series becomes summable, and this suggests that the underlying theory has a real positive spectrum.

Replacing conventional  $g\phi^4$  or  $g\phi^3$  theories by  $\mathcal{PT}$ -symmetric  $-g\phi^4$  or  $ig\phi^3$  theories has the effect of reversing signs in the beta function. Thus, theories that are not asymptotically free become asymptotically free and theories that lack stable critical points develop such points. There is evidence that  $-g\phi^4$  in four dimensions is nontrivial [8].

Supersymmetric quantum field theory that is  $\mathcal{PT}$  invariant has also been studied [9]. When we construct a two-dimensional supersymmetric quantum field theory by using a superpotential of the form  $\mathcal{S}(\phi) = -ig(i\phi)^{1+\epsilon}$ , the supersymmetric Lagrangian resulting from this superpotential is

$$\begin{aligned} \mathcal{L} &= \frac{1}{2}(\partial\phi)^2 + \frac{1}{2}i\bar{\psi}\not{\partial}\psi + \frac{1}{2}\mathcal{S}'(\phi)\bar{\psi}\psi + \frac{1}{2}[\mathcal{S}(\phi)]^2 \\ &= \frac{1}{2}(\partial\phi)^2 + \frac{1}{2}i\bar{\psi}\not{\partial}\psi + \frac{1}{2}g(1+\epsilon)(i\phi)^\epsilon\bar{\psi}\psi \\ &\quad - \frac{1}{2}g^2(i\phi)^{2+2\epsilon}, \end{aligned} \quad (1.6)$$

where  $\psi$  is a Majorana spinor. The Lagrangian (1.3) has a broken parity symmetry. This poses the question, Does the parity violation induce a breaking of supersymmetry? To answer this question, both the ground-state energy  $E_0$  and the fermion-boson mass ratio  $R$  were calculated as series in powers of the parameter  $\epsilon$ . Through second order in  $\epsilon$ ,  $E_0 = 0$  and  $R = 1$ , which strongly suggests that supersymmetry remains unbroken. We believe that these results are valid to all orders in powers of  $\epsilon$ . This work and our unpublished numerical studies of SUSY quantum mechanics show that complex deformations do not break supersymmetry.

Quantum field theories having the property of  $\mathcal{PT}$  invariance exhibit other interesting features. For example, the Ising limit of a  $\mathcal{PT}$ -invariant scalar quantum field theory is intriguing because it is dominated by solitons rather than by instantons as in a conventional quantum field theory [10]. In addition, a model of  $\mathcal{PT}$ -invariant quantum electrodynamics has been studied [11]. The massless theory exhibits a stable, nontrivial fixed point at which the renormalized theory is finite. Moreover, such a theory allows one to revive successfully the original electron model of Casimir.

Since  $\langle\phi\rangle \neq 0$  in  $\mathcal{PT}$ -symmetric theories, one can in principle calculate directly (using the Schwinger-Dyson equations, for example) the real positive Higgs mass in a renormalizable  $\mathcal{PT}$ -symmetric theory in which symmetry breaking occurs naturally. No symmetry-breaking parameter needs to be introduced. This most intriguing idea could lead to an experimental vindication of our proposed generalization of the notion of Hermiticity to  $\mathcal{PT}$  symmetry.

This paper is organized as follows: In Sec. II we study the classical version of the Hamiltonian in Eq. (1.1). The behavior of classical orbits reveals the nature of the phase transition at  $\epsilon = 0$ . Next, in Sec. III we analyze the quantum version of this Hamiltonian. We derive several asymptotic results regarding the behavior of the energy levels near the phase transition. In Sec. IV we discuss the classical and quantum properties of the broad class of  $\mathcal{PT}$ -symmetric Hamiltonians in Eq. (1.4) of which  $H$  in Eq. (1.1) is a special case. Finally, in Sec. V we study complex deformations of nonanalytic potentials.

## II. CLASSICAL THEORY

The classical equation of motion for a particle described by  $H$  in (1.1) is obtained from Hamilton's equations:

$$\begin{aligned} \frac{dx}{dt} &= \frac{\partial H}{\partial p} = 2p, \\ \frac{dp}{dt} &= -\frac{\partial H}{\partial x} = i(2 + \epsilon)(ix)^{1+\epsilon}. \end{aligned} \quad (2.1)$$

Combining these two equations gives

$$\frac{d^2x}{dt^2} = 2i(2 + \epsilon)(ix)^{1+\epsilon}, \quad (2.2)$$

which is the complex version of Newton's second law,  $F = ma$ .

Equation (2.2) can be integrated once to give [12]

$$\frac{1}{2} \frac{dx}{dt} = \pm \sqrt{E + (ix)^{2+\epsilon}}, \quad (2.3)$$

where  $E$  is the energy of the classical particle (the time-independent value of  $H$ ). We treat time  $t$  as a real variable that parameterizes the complex path  $x(t)$  of this particle.

This section is devoted to studying and classifying the solutions to Eq. (2.3). By virtue of the  $\mathcal{PT}$  invariance of the Hamiltonian  $H$ , it seems reasonable to restrict our attention to real values of  $E$ . Given this restriction, we can always rescale  $x$  and  $t$  by real numbers so that without loss of generality Eq. (2.3) reduces to

$$\frac{dx}{dt} = \pm \sqrt{1 + (ix)^{2+\epsilon}}. \quad (2.4)$$

The trajectories satisfying Eq. (2.4) lie on a multi-sheeted Riemann surface. On this surface the function  $\sqrt{1 + (ix)^{2+\epsilon}}$  is single-valued. There are two sets of branch cuts. The cuts in the first set radiate outward from the roots of

$$1 + (ix)^{2+\epsilon} = 0. \quad (2.5)$$

These roots are the classical turning points of the motion. There are many turning points, all lying at a distance of unity from the origin. The angular separation between consecutive turning points is  $2\pi/(2 + \epsilon)$ . The second set of branch cuts is present only when  $\epsilon$  is noninteger. In order to maintain explicit  $\mathcal{PT}$  symmetry (left-right symmetry in the complex- $x$  plane), we choose these branch cuts to run from the origin to infinity along the positive imaginary axis.

### A. Case $\epsilon = 0$

Because the classical solutions to Eq. (2.4) have a very elaborate structure, we begin by considering some special values of  $\epsilon$ . The simplest case is  $\epsilon = 0$ . For this case there are only two turning points and these lie on the real axis at  $\pm 1$ .

In order to solve Eq. (2.4) we need to specify an initial condition  $x(0)$ . The simplest choice for  $x(0)$  is a turning point. If the path begins at  $\pm 1$ , there is a unique direction in the complex- $x$  plane along which the phases of the left side and the right side of Eq. (2.4) agree. This gives rise to a trajectory on the real axis that oscillates between the two turning points. This is the well-known sinusoidal motion of the harmonic oscillator.

Note that once the turning points have been fixed the energy is determined. Thus, choosing the initial position of the particle determines the initial velocity (up to a plus or minus sign) as well. So, if the path of the particle begins anywhere on the real axis between the turning points, the initial velocity is fixed up to a sign and the trajectory of the particle still oscillates between the turning points.

Ordinarily, in conventional classical mechanics the only possible initial positions for the particle lie on the real axis between the turning points because the velocity is real; all other points on the real axis lie in the classically forbidden region. However, because we are analytically continuing classical mechanics into the complex plane, we can choose any point  $x(0)$  in the complex plane as an initial position. For all complex initial positions outside of the conventional classically allowed region the classical trajectory is an ellipse whose foci are the turning points. The ellipses are nested because no trajectories may cross. (See Fig. 1.) The exact solution to Eq. (2.4) is

$$x(t) = \cos[\arccos x(0) \pm t], \quad (2.6)$$

where the sign of  $t$  determines the direction (clockwise or anticlockwise) in which the particle traces the ellipse. For *any* ellipse the period of the motion is  $2\pi$ . The period is the same for all trajectories because we can join the square-root branch cuts emanating from the turning points, creating a single finite branch cut lying along the real axis from  $x = -1$  to  $x = 1$ . The complex path integral that determines the period can then be shrunk (by Cauchy's theorem) to the usual real integral joining the turning points.

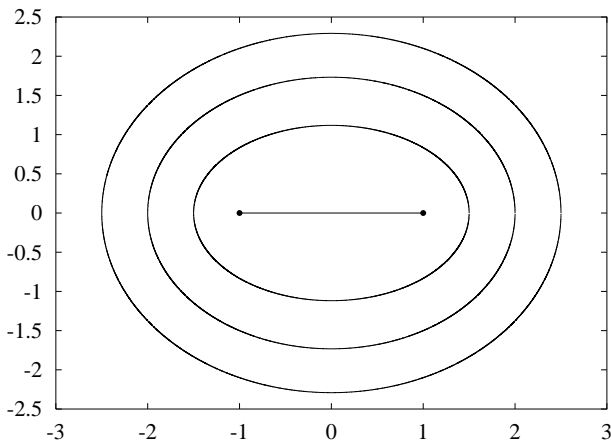


FIG. 1. Classical trajectories in the complex- $x$  plane for the harmonic oscillator whose Hamiltonian is  $H = p^2 + x^2$ . These trajectories represent the possible paths of a particle whose energy is  $E = 1$ . The trajectories are nested ellipses with foci located at the turning points at  $x = \pm 1$ . The real line segment (degenerate ellipse) connecting the turning points is the usual periodic classical solution to the harmonic oscillator. All closed paths [see Eq. (2.6)] have the same period  $2\pi$ .

Finally, we remark that all of the classical paths (elliptical orbits) are symmetric with respect to parity  $\mathcal{P}$  (reflections through the origin) and time reversal  $\mathcal{T}$  (reflections about the real axis), as well as  $\mathcal{PT}$  (reflections about the imaginary axis). Furthermore,  $\mathcal{P}$  and  $\mathcal{T}$  individually preserve the directions in which the ellipses are traversed.

## B. Case $\epsilon = 1$

The case  $\epsilon = 1$  is significantly more complicated. Now there are three turning points. Two are located below the real axis and these are symmetric with respect to the imaginary axis:  $x_- = e^{-5i\pi/6}$  and  $x_+ = e^{-i\pi/6}$ . That is, under  $\mathcal{PT}$  reflection  $x_-$  and  $x_+$  are interchanged. The third turning point lies on the imaginary axis at  $x_0 = i$ .

As in the case  $\epsilon = 0$ , the trajectory of a particle that begins at the turning point  $x_-$  follows a unique path in the complex- $x$  plane to the turning point at  $x_+$ . Then, the particle retraces its path back to the turning point at  $x_-$ , and it continues to oscillate between these two turning points. This path is shown on Fig. 2. The period of this motion is  $2\sqrt{3}\pi\Gamma(\frac{4}{3})/\Gamma(\frac{5}{6})$ . The periodic motion between  $x_{\pm}$  is clearly time-reversal symmetric.

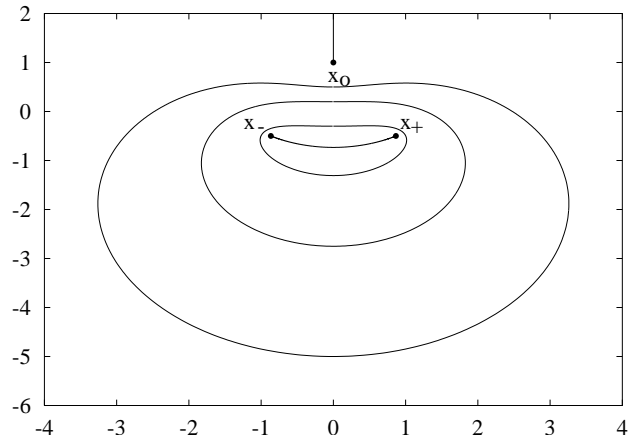


FIG. 2. Classical trajectories in the complex- $x$  plane for a particle described by the Hamiltonian  $H = p^2 + ix^3$  and having energy  $E = 1$ . An oscillatory trajectory connects the turning points  $x_{\pm}$ . This trajectory is enclosed by a set of closed, nested paths that fill the finite complex- $x$  plane except for points on the imaginary axis at or above the turning point  $x_0 = i$ . Trajectories originating at one of these exceptional points go off to  $i\infty$  or else they approach  $x_0$ , stop, turn around, and then move up the imaginary axis to  $i\infty$ .

A particle beginning at the third turning point  $x_0$  exhibits a completely distinct motion: It travels up the imaginary axis and reaches  $i\infty$  in a finite time  $\sqrt{\pi}\Gamma(\frac{4}{3})/\Gamma(\frac{5}{6})$ . This motion is not periodic and is not symmetric under time reversal.

Paths originating from all other points in the finite

complex- $x$  plane follow closed periodic orbits. No two orbits may intersect; rather they are all nested, like the ellipses for the case  $\epsilon = 0$ . All of these orbits encircle the turning points  $x_{\pm}$  and, by virtue of Cauchy's theorem, have the same period  $2\sqrt{3}\pi\Gamma(\frac{4}{3})/\Gamma(\frac{5}{6})$  as the oscillatory path connecting  $x_{\pm}$ . Because these orbits must avoid crossing the trajectory that runs up the positive imaginary axis from the turning point  $x_0 = i$ , they are pinched in the region just below  $x_0$ , as shown on Fig. 2.

As these orbits become larger they develop sharper indentations in the vicinity of  $x_0$ . We observe that the characteristic radius of a large orbit approaches the reciprocal of the distance  $d$  between  $x_0$  and the point where the orbit intersects the positive imaginary axis. Thus, it is appropriate to study these orbits from the point of view of the renormalization group: We scale the distance  $d$  down by a factor  $L$  and then plot the resulting orbit on a graph whose axis are scaled down by the same factor  $L$ . Repeated scaling gives a limiting orbit whose shape resembles a cardioid (see Fig. 3). The equation of this limiting orbit is obtained in the asymptotic regime where we neglect the dimensionless energy 1 in Eq. (2.4):

$$\frac{dx}{dt} = \pm(ix)^{3/2}. \quad (2.7)$$

The solution to this differential equation, scaled so that it crosses the negative imaginary axis at  $-3i$ , is

$$x(t) = \frac{4i}{(t + 2i/\sqrt{3})^2} \quad (-\infty < t < \infty). \quad (2.8)$$

This curve is shown as the solid line in Fig. 3. (Strictly speaking, this curve is not a true cardioid, but its shape so closely resembles a true cardioid that we shall refer to it in this paper as the *limiting cardioid*.)

In the infinite scaling limit all periodic orbits [all these orbits have period  $2\sqrt{3}\pi\Gamma(\frac{4}{3})/\Gamma(\frac{5}{6})$ ], which originally filled the entire finite complex- $x$  plane, have been squeezed into the region inside the limiting cardioid (2.8). The nonperiodic orbit still runs up the positive imaginary axis. The obvious question is, What complex classical dynamics is associated with all of the other points in the scaled complex- $x$  plane that lie outside of the limiting cardioid? We emphasize that all of these points were originally at infinity in the unscaled complex- $x$  plane.

We do not know the exact answer to this question, but we can draw a striking and suggestive analogy with some previously published work. It is generally true that the region of convergence in the complex- $x$  plane for an infinitely iterated function is a cardioid-shaped region. For example, consider the continued exponential function

$$f(x) = e^{xe^{xe^{\dots}}}. \quad (2.9)$$

The sequence  $e^x, e^{xe^x}, \dots$  is known to converge in a cardioid-shaped region of the complex- $x$  plane (see

Figs. 2-4 in Ref. [13]). It diverges on the straight line that emerges from the indentation of the cardioid. The remaining part of the complex- $x$  plane is divided into an extremely elaborate mosaic of regions in which this sequence converges to limit cycles of period 2, period 3, period 4, and so on. These regions have fractal structure. It would be interesting if unbounded complex classical motion exhibits this remarkable fractal structure. In other words, does the breaking of  $\mathcal{P}$  and  $\mathcal{T}$  symmetry allow for unbounded chaotic solutions?

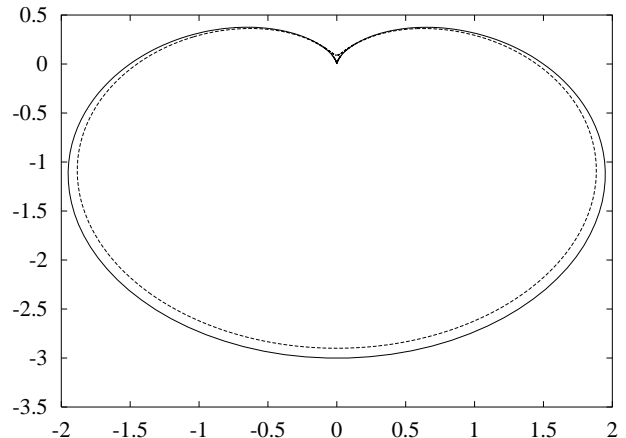


FIG. 3. Approach to the limiting cardioid in Eq. (2.8). As the orbits shown in Fig. 2 approach the turning point  $x_0$ , they get larger. Using a renormalization-group approach, we plot successively larger orbits (one such orbit is shown as a dashed line) scaled down by the characteristic size of the orbit. The limiting cardioid is indicated by a solid line. The indentation in the limiting cardioid develops because classical trajectories may not intersect and thus must avoid crossing the trajectory (shown in Fig. 2) on the imaginary axis above  $x_0$ .

### C. Case $\epsilon = 2$

When  $\epsilon = 2$  there are four turning points, two located below the real axis and symmetric with respect to the imaginary axis,  $x_1 = e^{-3i\pi/4}$  and  $x_2 = e^{-i\pi/4}$ , and two more located above the real axis and symmetric with respect to the imaginary axis,  $x_3 = e^{i\pi/4}$  and  $x_4 = e^{3i\pi/4}$ . Classical trajectories that oscillate between the pair  $x_1$  and  $x_2$  and the pair  $x_3$  and  $x_4$  are shown on Fig. 4. The period of these oscillations is  $2\sqrt{2}\pi\Gamma(\frac{5}{4})/\Gamma(\frac{3}{4})$ . Trajectories that begin elsewhere in the complex- $x$  plane are also shown on Fig. 4. Note that by virtue of Cauchy's theorem all these nested nonintersecting trajectories have the same period. All motion is periodic except for trajectories that begin on the real axis; a particle that begins on the real- $x$  axis runs off to  $\pm\infty$ , depending on the sign of the initial velocity. These are the only trajectories that are nonperiodic.

The rescaling argument that gives the cardioid for the case  $\epsilon = 1$  yields a doubly-indented cardioid for the case

$\epsilon = 2$  (see Fig. 5). This cardioid is similar to that in Fig. 5 of Ref. [13]. However, for the case  $\epsilon = 2$  the limiting double cardioid consists of two perfect circles, which are tangent to one another at the origin  $x = 0$ . Circles appear because at  $\epsilon = 2$  in the scaling limit the equation corresponding to (2.7) is  $\frac{dx}{dt} = \pm x^2$ . The solutions to this equation are the inversions  $x(t) = \pm \frac{1}{t+i}$ , which map the real- $t$  axis into circles in the complex- $x$  plane.

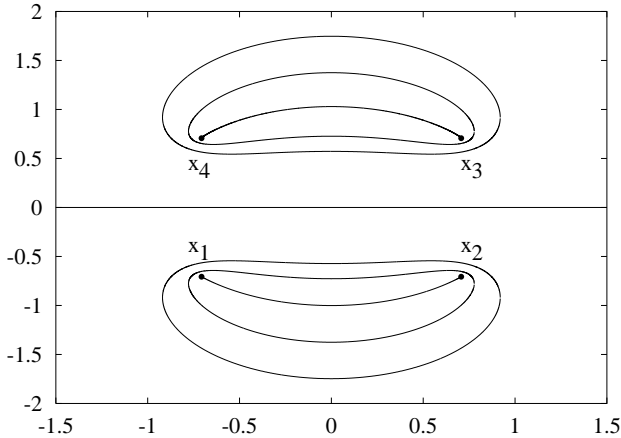


FIG. 4. Classical trajectories in the complex- $x$  plane for a particle described by the Hamiltonian  $H = p^2 - x^4$  and having energy  $E = 1$ . There are two oscillatory trajectories connecting the pairs of turning points  $x_1$  and  $x_2$  in the lower-half  $x$ -plane and  $x_3$  and  $x_4$  in the upper-half  $x$ -plane. [A trajectory joining any other pair of turning points is forbidden because it would violate  $\mathcal{PT}$  (left-right) symmetry.] The oscillatory trajectories are surrounded by closed orbits of the same period. In contrast to these periodic orbits there is a class of trajectories having unbounded path length and running along the real- $x$  axis. These are the only paths that violate time-reversal symmetry.

#### D. Case $\epsilon = 5$

When  $\epsilon = 5$  there are seven turning points, one located at  $i$  and three pairs, each pair symmetric with respect to reflection about the imaginary axis ( $\mathcal{PT}$  symmetric). We find that each of these pairs of turning points is joined by an oscillatory classical trajectory. (A trajectory joining any other two turning points would violate  $\mathcal{PT}$  symmetry.) Surrounding each of the oscillatory trajectories are nested closed loops, each loop having the same period as the oscillatory trajectory it encloses. These classical trajectories are shown on Fig. 6. The periods for these three families of trajectories are

$$4\sqrt{\pi} \frac{\Gamma(8/7)}{\Gamma(9/14)} \cos \theta,$$

where  $\theta = 5\pi/14$  for the lowest pair of turning points,  $\theta = \pi/14$  for the middle pair, and  $\theta = 3\pi/14$  for the pair above the real axis.

One other class of trajectory is possible. If the initial position of the classical particle lies on the imaginary axis at or above the turning point at  $i$ , then depending on the sign of the initial velocity, the particle either runs off to  $i\infty$  or it approaches the turning point, reverses its direction, and then goes off to  $i\infty$ . These purely imaginary paths are the only possible nonperiodic trajectories. They are also shown on Fig. 6.

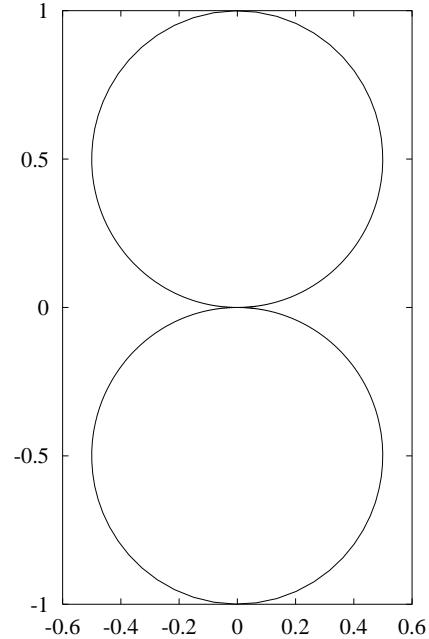


FIG. 5. Limiting double cardioid for the case  $\epsilon = 2$ . As the orbits in Fig. 4 approach the real axis, they get larger. If we scale successively larger orbits down by their characteristic size, then in the limiting case the orbits approach two circles tangent at the origin. In this limit the four turning points in Fig. 4 coalesce at the point of tangency.

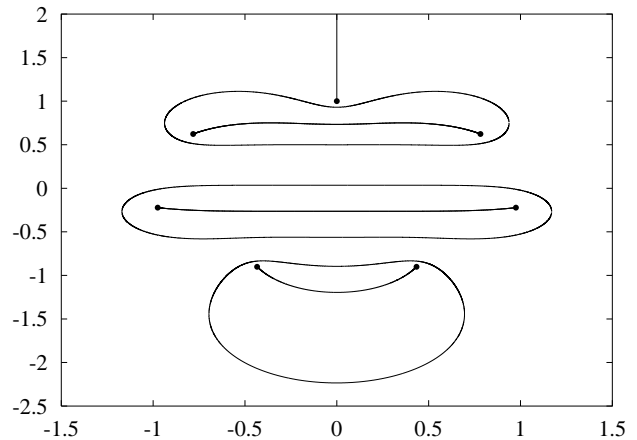


FIG. 6. Classical trajectories in the complex- $x$  plane for a particle described by the Hamiltonian  $H = p^2 + ix^7$  and having energy  $E = 1$ . Shown are oscillatory trajectories surrounded by periodic trajectories. Unbounded trajectories run along the positive-imaginary axis above  $x = i$ .

### E. General case: Noninteger values of $\epsilon > 0$

Because Eq. (2.4) contains a square-root function, the turning points, which are solutions to Eq. (2.5), are square-root branch points for all values of  $\epsilon$ . Thus, in principle, the complex trajectories  $x(t)$  lie on a multi-sheeted Riemann surface. However, when  $\epsilon$  is a nonnegative integer, we can define the branch cuts so that the classical trajectories satisfying Eq. (2.4) never leave the principal sheet of this Riemann surface. We do this as follows: We choose to join the  $\mathcal{PT}$ -symmetric (left-right-symmetric) pairs of turning points by branch cuts that follow exactly the oscillatory solutions connecting these pairs. (There are three such pairs in Fig. 6, two in Fig. 4, and one in Figs. 2 and 1.) If  $\epsilon$  is odd, there is one extra turning point that lies on the positive imaginary axis (see Figs. 2 and 6); the branch cut emanating from this turning point runs up the imaginary- $x$  axis to  $i\infty$ . Since classical paths never cross, there are no trajectories that leave the principal sheet of the Riemann surface.

When  $\epsilon$  is noninteger, we can see from the argument of the square-root function in Eq. (2.4) that there is an entirely new branch cut, which emerges from the origin in the complex- $x$  plane. To preserve  $\mathcal{PT}$  symmetry we choose this branch cut to run off to  $\infty$  along the positive-imaginary  $x$ -axis. If  $\epsilon$  is rational, the Riemann surface has a finite number of sheets, but if  $\epsilon$  is irrational, then there are an infinite number of sheets.

If a classical trajectory crosses the branch cut emanating from the origin, then this trajectory leaves the principal sheet of the Riemann surface. In Fig. 7 we illustrate some of the possible classical trajectories for the case  $\epsilon = \pi - 2$ . The top plot shows some trajectories that do not cross the positive-imaginary  $x$ -axis and thus do not leave the principal sheet of the Riemann surface. The trajectories shown are qualitatively similar to those in Fig. 2; all trajectories have the same period.

In the middle plot of Fig. 7 is a trajectory that crosses the positive-imaginary  $x$ -axis and visits *three* sheets of the Riemann surface. The solid line and the dotted line outside of the solid line lie on the principal sheet, while the remaining two portions of the dotted line lie on two other sheets. Note that this trajectory does *not* cross itself; we have plotted the projection of the trajectory onto the principal sheet. The trajectory continues to exhibit  $\mathcal{PT}$  symmetry. The period of the trajectory is greater than that of the period of the trajectories shown in the top plot. This is because the trajectory encloses turning points that are not on the principal sheet. In general, as the size of the trajectory increases, it encloses more and more complex turning points; each time a new pair of turning points is surrounded by the trajectory the period jumps by a discrete quantity.

Although the trajectory in the bottom plot in Fig. 7 has the same topology as that in the middle plot, it is

larger. As the trajectory continues to grow, we observe a phenomenon that seems to be universal; namely, the appearance of a limiting cardioid shape (solid line) on the principal surface. The remaining portion of the trajectory (dotted line) shrinks relative to the cardioid and becomes compact and knot-like.

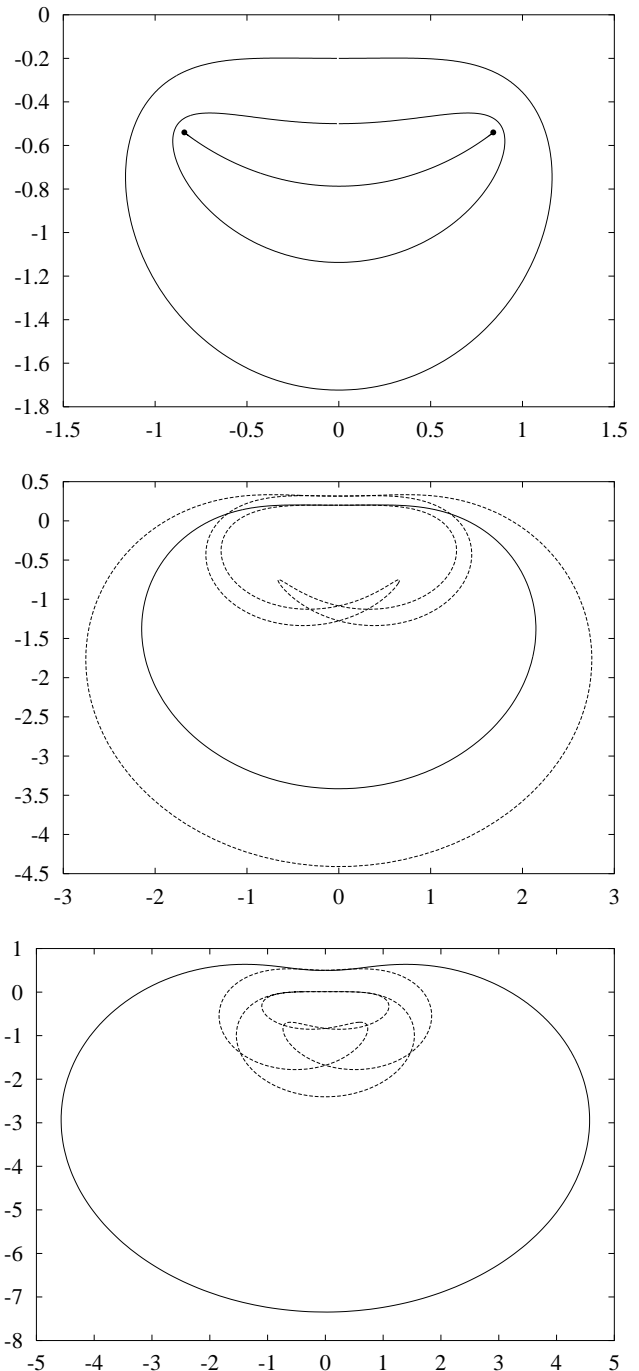


FIG. 7. Classical trajectories for  $H = p^2 - (ix)^\pi$  corresponding to the case  $\epsilon = \pi - 2$ . Observe that as the classical trajectory increases in size, a limiting cardioid appears on the principal sheet of the Riemann surface. On the other sheets the trajectory becomes relatively small and knot-like.

In Fig. 8 we examine the case  $\epsilon = 0.5$ . In this figure we observe behavior that is qualitatively similar to that seen in Fig. 7; namely, as the trajectory on the principal sheet of the Riemann surface becomes larger and approaches a limiting cardioid, the remaining portion of the trajectory becomes relatively small and knot-like.

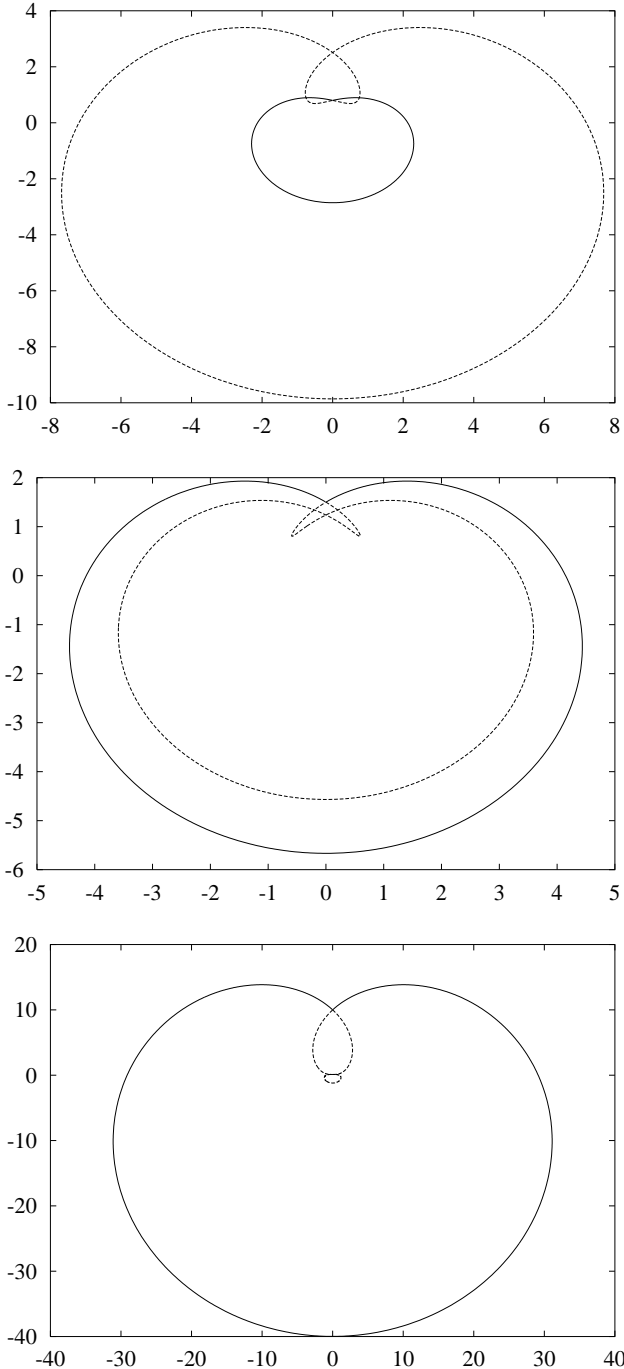


FIG. 8. Classical trajectories for the case  $\epsilon = 0.5$ . As the classical path on the principal sheet of the Riemann surface increases in size it approaches a limiting cardioid, just as in Fig. 7. The remaining portion of the path becomes relatively small and knot-like.

To summarize, for any  $\epsilon > 0$  the classical paths are always  $\mathcal{PT}$  symmetric. The simplest such path describes oscillatory motion between the pair of turning points that lie just below the real axis on the principal sheet. In general, the period of this motion as a function of  $\epsilon$  is given by

$$T = 4\sqrt{\pi}E^{-\frac{\epsilon}{4+2\epsilon}} \frac{\Gamma\left(\frac{3+\epsilon}{2+\epsilon}\right)}{\Gamma\left(\frac{4+\epsilon}{4+2\epsilon}\right)} \cos\left(\frac{\epsilon\pi}{4+2\epsilon}\right). \quad (2.10)$$

Other closed paths having more complicated topologies (and longer periods) also exist, as shown in Figs. 7 and 8.

Whenever the classical motion is periodic, we expect the quantized version of the theory to exhibit real eigenvalues. Although we have not yet done so, we intend to investigate the consequences of quantizing a theory whose underlying classical paths have complicated topological structures traversing several sheets of a Riemann surface. The properties of such a theory of quantum knots might well be novel.

#### F. Case $-1 < \epsilon < 0$

Classical paths for negative values of  $\epsilon$  are fundamentally different from those corresponding to nonnegative values of  $\epsilon$ ; such paths no longer exhibit  $\mathcal{PT}$  symmetry. Furthermore, we no longer see paths that are periodic; all paths eventually spiral outwards to infinity. In general, the time that it takes for a particle to reach infinity is infinite.

We interpret the abrupt change in the global nature of the classical behavior that occurs as  $\epsilon$  passes through 0 as a change in phase. For all values of  $\epsilon$  the Hamiltonian in Eq. (1.1) is  $\mathcal{PT}$  (left-right) symmetric. However, for  $\epsilon < 0$  the solutions cease to exhibit  $\mathcal{PT}$  symmetry. Thus, we say that  $\epsilon \geq 0$  is a  $\mathcal{PT}$ -symmetric phase and that  $\epsilon < 0$  is a spontaneously broken  $\mathcal{PT}$ -symmetric phase.

To illustrate the loss of  $\mathcal{PT}$  (left-right) symmetry, we plot in Fig. 9 the classical trajectory for a particle that starts at a turning point  $x_- = -\pi\frac{4+\epsilon}{4+2\epsilon}$  in the second quadrant of the complex- $x$  plane ( $\text{Re } x < 0, \text{Im } x > 0$ ) for three values of  $\epsilon$ :  $-0.2, -0.15,$  and  $-0.1$ . We observe that a path starting at this turning point moves toward but *misses* the  $\mathcal{PT}$ -symmetric turning point  $x_+ = -\pi\frac{\epsilon}{4+2\epsilon}$  because it crosses the branch cut on the positive-imaginary  $x$ -axis. This path spirals outward, crossing from sheet to sheet on the Riemann surface, and eventually veers off to infinity asymptotic to the angle  $\theta_\infty$ , where

$$\theta_\infty = -\frac{2+\epsilon}{2\epsilon}\pi. \quad (2.11)$$

This formula shows that the total angular rotation of the spiral is finite for all  $\epsilon \neq 0$  but becomes infinite as



$\epsilon \rightarrow 0^-$ . In the top figure ( $\epsilon = -0.2$ ) the spiral makes  $2\frac{1}{4}$  turns before moving off to infinity; in the middle figure ( $\epsilon = -0.15$ ) the spiral makes  $3\frac{1}{12}$  turns; in the bottom figure ( $\epsilon = -0.1$ ) the spiral makes  $4\frac{3}{4}$  turns.

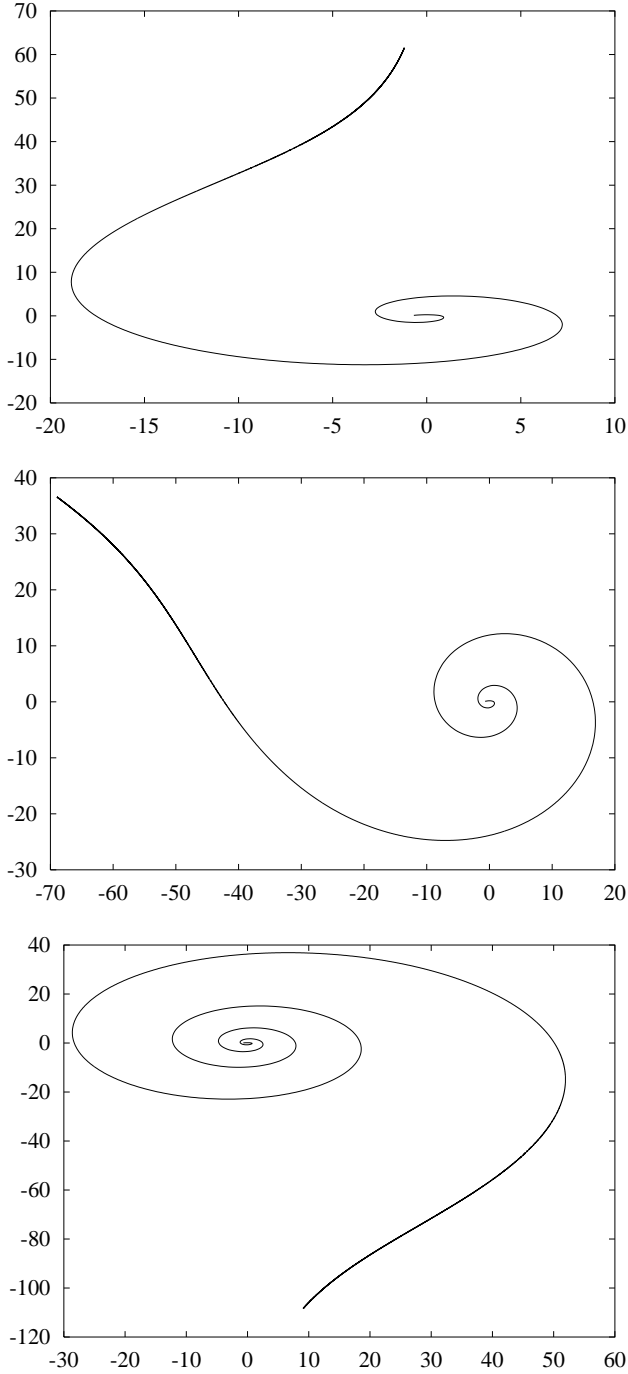


FIG. 9. Classical trajectories that violate  $\mathcal{PT}$  symmetry. The top plot corresponds to the case  $\epsilon = -0.2$ , the middle plot to  $\epsilon = -0.15$ , and the bottom plot to  $\epsilon = -0.1$ . The paths in each plot begin at a turning point and spiral outwards to infinity in an infinite amount of time.

Note that the spirals in Fig. 9 pass many classical

turning points as they spiral clockwise from  $x_-$ . [From Eq. (2.5) we see that the  $n$ th turning point lies at the angle  $\frac{4-\epsilon-4n}{4+2\epsilon}\pi$  ( $x_-$  corresponds to  $n = 0$ ).] As  $\epsilon$  approaches 0 from below, when the classical trajectory passes a new turning point, there is a corresponding merging of the quantum energy levels as shown in Fig. 11. As pointed out in Ref. [1], this correspondence becomes exact in the limit  $\epsilon \rightarrow 0^-$  and is a manifestation of Ehrenfest's theorem.

### G. Case $\epsilon = -1$

For this special case we can solve the equation (2.4) exactly. The result,

$$x(t) = \left(1 - b^2 + \frac{1}{4}t^2\right)i + bt \quad (b \text{ real}), \quad (2.12)$$

represents a family of parabolas that are symmetric with respect to the imaginary axis (see Fig. 10). Note that there is one degenerate parabola corresponding to  $b = 0$  that lies on the positive imaginary axis above  $i$ .

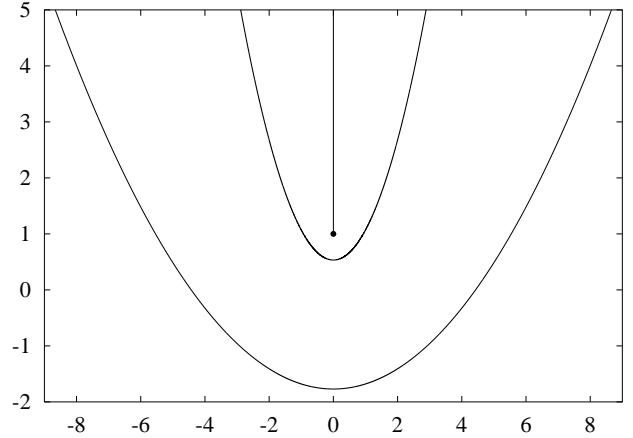


FIG. 10. Classical trajectories in the complex- $x$  plane for a particle described by the Hamiltonian  $H = p^2 - ix$  and having energy  $E = 1$ . Shown are parabolic trajectories and a turning point at  $i$ . All trajectories are unbounded.

## III. QUANTUM THEORY

In this section we discuss the quantum properties of the Hamiltonian  $H$  in Eq. (1.1). The spectrum of this Hamiltonian is obtained by solving the corresponding Schrödinger equation

$$-\psi''(x) + [x^2(ix)^\epsilon - E]\psi(x) = 0 \quad (3.1)$$

subject to appropriate boundary conditions imposed in the complex- $x$  plane. These boundary conditions are described in Ref. [1]. A plot of the spectrum of  $H$  is shown in Fig. 11.

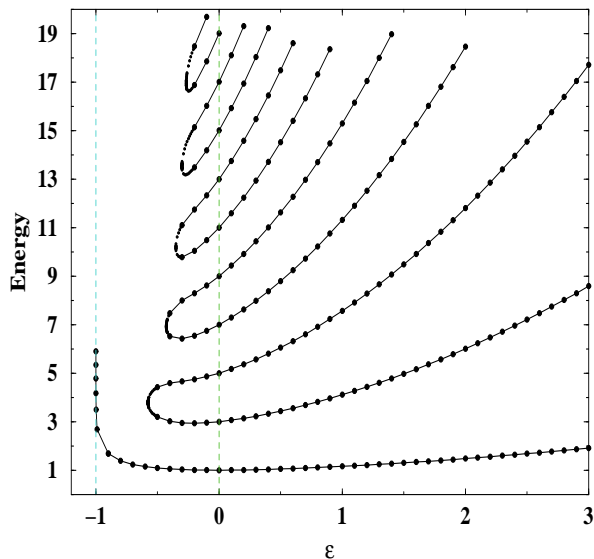


FIG. 11. Energy levels of the Hamiltonian  $H = p^2 + x^2(ix)^\epsilon$  as a function of the parameter  $\epsilon$ . There are three regions: When  $\epsilon \geq 0$ , the spectrum is real and positive and the energy levels rise with increasing  $\epsilon$ . The lower bound of this region,  $\epsilon = 0$ , corresponds to the harmonic oscillator, whose energy levels are  $E_n = 2n + 1$ . When  $-1 < \epsilon < 0$ , there are a finite number of real positive eigenvalues and an infinite number of complex conjugate pairs of eigenvalues. As  $\epsilon$  decreases from 0 to  $-1$ , the number of real eigenvalues decreases; when  $\epsilon \leq -0.57793$ , the only real eigenvalue is the ground-state energy. As  $\epsilon$  approaches  $-1^+$ , the ground-state energy diverges. For  $\epsilon \leq -1$  there are no real eigenvalues.

There are several ways to obtain the spectrum that is displayed in Fig. 11. The simplest and most direct technique is to integrate the differential equation using Runge-Kutta. To do so, we convert the complex differential equation (3.1) to a system of coupled, real, second-order equations. We find that the convergence is most rapid when we integrate along anti-Stokes lines and then patch the two solutions together at the origin. This procedure, which is described in Ref. [1], gives highly accurate numerical results.

To verify the Runge-Kutta approach, we have solved the differential equation (3.1) using an independent and alternative procedure. We construct a matrix representation of the Hamiltonian in Eq. (1.1) in harmonic oscillator basis functions  $e^{-x^2/2} H_n(x) \pi^{-1/4} / \sqrt{2^n n!}$ :

$$M_{m,n} = - \int_{-\infty}^{\infty} dx \frac{1}{\sqrt{\pi 2^{m+n} m! n!}} e^{-x^2/2} H_m(x) \times \left\{ \frac{d^2}{dx^2} - i^{m+n} \cos \left[ \frac{\pi}{2} (\epsilon - m - n) \right] |x|^{2+\epsilon} \right\} \times e^{-x^2/2} H_n(x). \quad (3.2)$$

The  $K$ -th approximant to the spectrum comes from diagonalizing a truncated version of this matrix  $M_{m,n}$  ( $0 \leq m, n \leq K$ ). One drawback of this method is that

the eigenvalues of  $M_{m,n}$  approximate those of the Hamiltonian  $H$  in (1.1) only if  $-1 < \epsilon < 2$ . Another drawback is that the convergence to the exact eigenvalues is slow and not monotone because the Hamiltonian  $H$  is not Hermitian in a conventional sense. We illustrate the convergence of this truncation and diagonalization procedure for  $\epsilon = -\frac{1}{2}$  in Fig. 12.

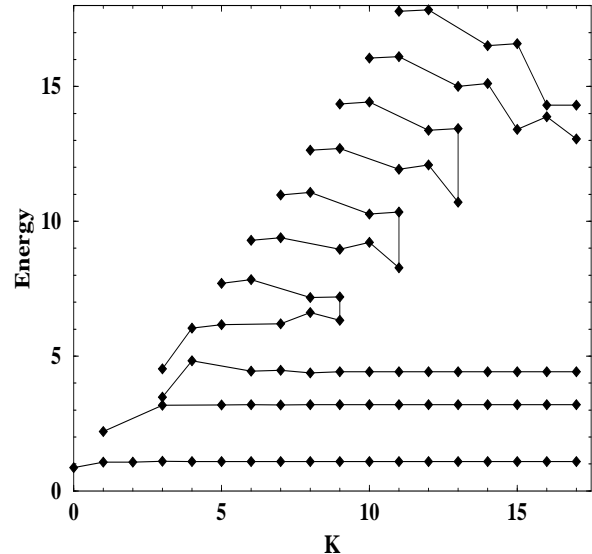


FIG. 12. Real eigenvalues of the  $(K + 1) \times (K + 1)$  truncated matrix  $M_{m,n}$  in Eq. (3.2) ( $K = 0, 1, \dots, 17$ ) for  $\epsilon = -1/2$ . As  $K$  increases, the three lowest eigenvalues converge to the three real energy levels in Fig. 11 at  $\epsilon = -1/2$ . The other real eigenvalues do not stabilize, and instead disappear in pairs.

A third method for finding the eigenvalues in Fig. 11 is to use WKB. Complex WKB theory (see Eq. 5.4) gives an excellent analytical approximation to the spectrum.

In the next two subsections we examine two aspects of the spectrum in Fig. 11. First, we study the asymptotic behavior of the ground-state energy as  $\epsilon \rightarrow -1$ . Second, we examine the phase transition in the vicinity of  $\epsilon = 0$ .

### A. Behavior of the ground-state energy near $\epsilon = -1$

In this subsection we give an analytic derivation of the behavior of the lowest real energy level in Fig. 11 as  $\epsilon \rightarrow -1$ . We show that in this limit the eigenvalue grows logarithmically.

When  $\epsilon = -1$ , the differential equation (3.1) reduces to

$$-\psi''(x) - ix\psi(x) = E\psi(x), \quad (3.3)$$

which can be solved exactly in terms of Airy functions [14]. The anti-Stokes lines at  $\epsilon = -1$  lie at  $30^\circ$  and at  $-210^\circ$  in the complex- $x$  plane. We find the solution that

vanishes exponentially along each of these rays and then rotate back to the real- $x$  axis to obtain

$$\psi_{L,R}(x) = C_{L,R} \text{Ai} \left( \mp x e^{\pm i\pi/6} + E e^{\pm 2i\pi/3} \right). \quad (3.4)$$

We must patch these solutions together at  $x = 0$  according to the patching condition

$$\frac{d}{dx} |\psi(x)|^2 \Big|_{x=0} = 0. \quad (3.5)$$

But for real  $E$ , the Wronskian identity for the Airy function [14] is

$$\frac{d}{dx} \left| \text{Ai} \left( x e^{-i\pi/6} + E e^{-2i\pi/3} \right) \right|^2 \Big|_{x=0} = -\frac{1}{2\pi} \quad (3.6)$$

instead of 0. Hence, there is no real eigenvalue.

Next, we perform an asymptotic analysis for  $\epsilon = -1 + \delta$  where  $\delta$  is small and positive:

$$\begin{aligned} -\psi''(x) - (ix)^{1+\delta} \psi(x) &= E \psi(x), \\ \psi(x) &\sim y_0(x) + \delta y_1(x) + \mathcal{O}(\delta^2) \quad (\delta \rightarrow 0+). \end{aligned} \quad (3.7)$$

We assume that  $E \rightarrow \infty$  as  $\delta \rightarrow 0+$  and obtain

$$\begin{aligned} y_0''(x) + ix y_0(x) + E y_0(x) &= 0, \\ y_1''(x) + ix y_1(x) + E y_1(x) &= -ix \ln(ix) y_0(x), \end{aligned} \quad (3.8)$$

and so on.

To leading order we again obtain the Airy equation (3.3) for  $y_0(x)$ . The solution for  $y_0(x)$  ( $x \geq 0$ ) is given by  $\psi_R(x)$  in Eq. (3.4) and we are free to choose  $C_R = 1$ . We can expand the Airy function in  $y_0(x)$  for large argument in the limit  $E \rightarrow \infty$ :

$$\begin{aligned} y_0(x) &= \text{Ai} \left( x e^{-i\pi/6} + E e^{-2i\pi/3} \right) \\ &\sim \left( x e^{-i\pi/6} + E e^{-2i\pi/3} \right)^{-1/4} \\ &\quad \times \exp \left[ \frac{2}{3} \left( x e^{-i\pi/6} + E e^{-2i\pi/3} \right)^{3/2} \right]. \end{aligned} \quad (3.9)$$

At  $x = 0$  we get

$$\begin{aligned} y_0(0) &= \text{Ai}(E e^{-2i\pi/3}) \\ &\sim e^{i\pi/6} E^{-1/4} e^{\frac{2}{3} E^{3/2}} / (2\sqrt{\pi}). \end{aligned} \quad (3.10)$$

To next order in  $\epsilon$  we simplify the differential equation for  $y_1(x)$  in (3.8) by substituting

$$y_1(x) = Q(x) y_0(x). \quad (3.11)$$

Using the differential equation for  $y_0(x)$  in (3.8), we get

$$y_0(x) Q''(x) + 2y_0'(x) Q'(x) = -ix \ln(ix) y_0(x). \quad (3.12)$$

Multiplying this equation by the integrating factor  $y_0(x)$ , we obtain

$$[y_0^2(x) Q'(x)]' = -ix \ln(ix) y_0^2(x), \quad (3.13)$$

which integrates to

$$Q'(x) = \frac{i}{y_0^2(x)} \int_x^\infty dt t \ln(it) y_0^2(t), \quad (3.14)$$

where the upper limit of the integral ensures that  $Q'(x)$  is bounded for  $x \rightarrow \infty$ . Thus, we obtain

$$Q'(0) = \frac{i}{y_0^2(0)} \int_0^\infty dx x \ln(ix) y_0^2(x). \quad (3.15)$$

To determine the asymptotic behavior of the ground-state eigenvalue as  $\delta \rightarrow 0$ , we insert

$$\begin{aligned} \psi(x) &\sim y_0(x) + \delta y_1(x) + \mathcal{O}(\delta^2) \\ &= y_0(x) [1 + \delta Q(x)] + \mathcal{O}(\delta^2) \end{aligned} \quad (3.16)$$

into the quantization condition:

$$\begin{aligned} 0 &= \frac{d}{dx} [\psi^*(x) \psi(x)] \Big|_{x=0} \\ &\sim \frac{d}{dx} [|y_0(x)|^2 (1 + \delta Q^*(x)) (1 + \delta Q(x))] \Big|_{x=0} \\ &\sim \frac{d}{dx} [|y_0(x)|^2] \Big|_{x=0} + 2\delta |y_0(0)|^2 \text{Re}[Q'(0)] \\ &\quad + 2\delta \frac{d}{dx} [|y_0(x)|^2] \Big|_{x=0} \text{Re}[Q(0)]. \end{aligned} \quad (3.17)$$

We are free to choose  $Q(0) = 0$ , and doing so eliminates the last term on the right side. The leading-order result for the quantization condition in Eq. (3.6) then gives

$$\frac{1}{2\pi} \sim 2\delta |y_0(0)|^2 \text{Re}[Q'(0)]. \quad (3.18)$$

Next, we substitute the asymptotic form for  $y_0$  in Eq. (3.10) and the result for  $Q'(0)$  in Eq. (3.15) and obtain

$$\sqrt{E} e^{-\frac{4}{3} E^{3/2}} \sim 2\delta \text{Re} \int_0^\infty dx ix \ln(ix) \left[ \frac{y_0(x)}{y_0(0)} \right]^2. \quad (3.19)$$

Because the ratio of the unperturbed wave functions in the integrand in Eq. (3.19) is bounded and vanishes exponentially for large  $x$ , we know that the integral can grow at most as a power of  $E$ . Thus,

$$\delta \sim C E^\alpha e^{-\frac{4}{3} E^{3/2}} \quad (3.20)$$

for some power  $\alpha$  and constant  $C$  and the controlling behavior of the ground-state energy as  $\delta \rightarrow 0$  is given by

$$E \sim \left[ -\frac{3}{4} \ln \delta \right]^{\frac{2}{3}}, \quad (3.21)$$

where we have neglected terms that vary at most like  $\ln(\ln \delta)$ . Equation (3.21) gives the asymptotic behavior of the lowest energy level and is the result that we have sought. This asymptotic behavior is verified numerically in Table I.

## B. Behavior of energy levels near $\epsilon = 0$

In this subsection we examine analytically the phase transition that occurs at  $\epsilon = 0$ . In particular, we study high-lying eigenvalues for small negative values of  $\epsilon$  and verify that adjacent pairs of eigenvalues pinch off and become complex.

For small  $\epsilon$  we approximate  $H$  in Eq. (1.1) to first order in  $\epsilon$ :

$$H = p^2 + x^2 + \epsilon x^2 \ln(ix) + \mathcal{O}(\epsilon^2). \quad (3.22)$$

Using the identity  $\ln(ix) = \ln(|x|) + \frac{1}{2}i\pi \operatorname{sgn}(x)$ , we then have

$$H = p^2 + x^2 + \epsilon x^2 \left[ \ln(|x|) + \frac{i\pi}{2} \operatorname{sgn}(x) \right] + \mathcal{O}(\epsilon^2). \quad (3.23)$$

The simplest way to continue is to truncate this approximate Hamiltonian to a  $2 \times 2$  matrix. We introduce a harmonic oscillator basis as follows: The  $n$ th eigenvalue of the harmonic oscillator Hamiltonian  $p^2 + x^2$  is  $E_n = 2n + 1$  and the corresponding  $x$ -space normalized eigenstate  $|n\rangle$  is

$$\psi_n(x) = \frac{\pi^{-1/4}}{\sqrt{2^n n!}} e^{-x^2/2} H_n(x), \quad (3.24)$$

where  $H_n(x)$  is the  $n$ th Hermite polynomial [ $H_0(x) = 1$ ,  $H_1(x) = 2x$ ,  $H_2(x) = 4x^2 - 2$ ,  $H_3(x) = 8x^3 - 12x$ , and so on]. We then have the following diagonal matrix elements:

$$\langle n | p^2 + x^2 | n \rangle = 2n + 1, \quad (3.25)$$

$$\langle n | x^2 \ln(|x|) | n \rangle = a_n - \left( \frac{\gamma}{2} + \ln 2 \right) \left( n + \frac{1}{2} \right), \quad (3.26)$$

where  $\gamma$  is Euler's constant and

$$a_n = n + 1 + [n/2] + (n + 1/2) \sum_0^{[n+1/2]} \frac{1}{2k-1}. \quad (3.27)$$

We also have the off-diagonal matrix element

TABLE I. Comparison of the exact ground-state energy  $E$  near  $\epsilon = -1$  and the asymptotic results in Eq. (3.21). The explicit dependence of  $E$  on  $\epsilon = -1 + \delta$  is roughly  $E \propto (-\ln \delta)^{2/3}$  as  $\delta \rightarrow 0+$ .

$\delta$	$E_{\text{exact}}$	Eq. (3.21)
0.1	1.6837	2.0955
0.01	2.6797	2.9624
0.001	3.4947	3.6723
0.0001	4.1753	4.3013
0.00001	4.7798	4.8776
0.000001	5.3383	5.4158
0.0000001	5.8943	5.9244

$$\begin{aligned} & \langle 2n-1 | \frac{1}{2} i \pi x^2 \operatorname{sgn}(x) | 2n \rangle \\ &= \frac{1}{3} i (8n+1) \left[ \frac{\Gamma^2(n+1/2)}{n!(n-1)!} \right]^{1/2}. \end{aligned} \quad (3.28)$$

In the  $(2n-1) - (2n)$  subspace, the matrix  $H - E$  then reduces to the following  $2 \times 2$  matrix:

$$\begin{pmatrix} A - E & iB \\ iB & C - E \end{pmatrix}, \quad (3.29)$$

where for large  $n$  and small  $\epsilon$  we have

$$\begin{aligned} A &\sim 4n - 1 + \epsilon(n - 1/2) \ln(2n), \\ B &\sim \frac{8}{3} \epsilon n, \\ C &\sim 4n + 1 + \epsilon n \ln(2n). \end{aligned} \quad (3.30)$$

The determinant of the matrix in Eq. (3.29) gives the following roots for  $E$ :

$$E = \frac{1}{2} \left( A + C \pm \sqrt{(A - C)^2 - 4B^2} \right). \quad (3.31)$$

We observe that the roots  $E$  are degenerate when the discriminant (the square-root) in Eq. (3.31) vanishes. This happens when the condition

$$\epsilon = \frac{3}{8n} \quad (3.32)$$

is met. Hence, the sequence of points in Fig. 11 where the eigenvalues pinch off approaches  $\epsilon = 0$  as  $n \rightarrow \infty$ . For example, Eq. (3.32) predicts (using  $n = 4$ ) that  $E_7$  and  $E_8$  become degenerate and move off into the complex plane at  $\epsilon \approx -0.1$ . In Fig. 13 we compare our prediction for the behavior of  $E$  in Eq. (3.31) with a blow-up of a small portion of Fig. 11. We find that while our prediction is qualitatively good, the numerical accuracy is not particularly good. The lack of accuracy is not associated with truncating the expansion in powers of  $\epsilon$  but rather with truncating the Hamiltonian  $H$  to a  $2 \times 2$  matrix. Our numerical studies indicate that as the size of the matrix truncation increases, we obtain more accurate approximations to the behavior of the energy levels  $E$  in Fig. 11.

## IV. MORE GENERAL CLASSES OF THEORIES

In this section we generalize the results of Secs. II and III to a much wider class of theories. In particular, we consider a complex deformation of the  $x^{2K}$  anharmonic oscillator, where  $K = 1, 2, 3, \dots$  [see Eq. (1.4)]. The Schrödinger equation for this oscillator has the form

$$-\psi''(x) + [x^{2K}(ix)^\epsilon - E]\psi(x) = 0. \quad (4.1)$$

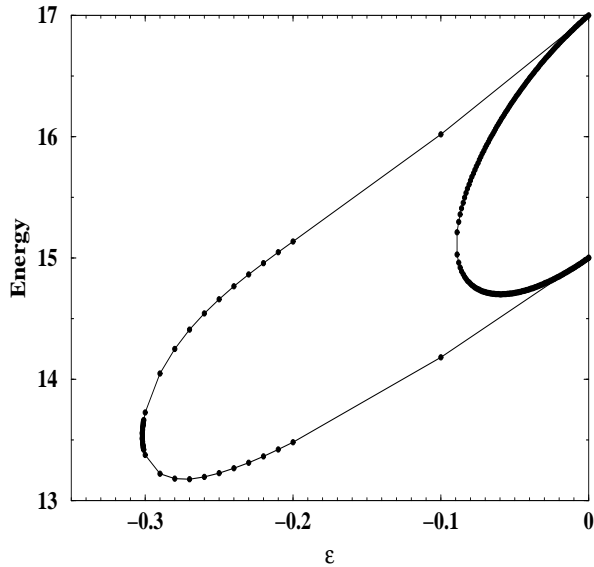


FIG. 13. A comparison of the prediction in Eq. (3.31) and a magnification of Fig. 11. Our prediction for the point at which  $E_7$  and  $E_8$  become degenerate is not very accurate numerically but is qualitatively quite good.

To determine the energy levels  $E$  as functions of the deformation parameter  $\epsilon$ , we must impose appropriate boundary conditions on Eq. (4.1). We require that the wave function vanish as  $|x| \rightarrow \infty$  inside of two wedges symmetrically placed about the imaginary- $x$  axis. The right wedge is centered about the angle  $\theta_{\text{right}}$ , where

$$\theta_{\text{right}} = -\frac{\epsilon\pi}{4K + 2\epsilon + 4}, \quad (4.2)$$

and the left wedge is centered about the angle  $\theta_{\text{left}}$ , where

$$\theta_{\text{left}} = -\pi + \frac{\epsilon\pi}{4K + 2\epsilon + 4}. \quad (4.3)$$

The opening angle of each of these wedges is

$$\frac{2\pi}{2K + \epsilon + 2}. \quad (4.4)$$

This pair of wedges is  $\mathcal{PT}$  (left-right) symmetric.

The orientation of these wedges is determined by analytically continuing the differential equation eigenvalue problem (4.1) and associated boundary conditions in the variable  $\epsilon$  using the techniques explained in Ref. [15]. The rotation of the boundary conditions is obtained from the asymptotic behavior of the solution  $\psi(x)$  for large  $|x|$ :

$$\psi(x) \sim \exp\left(\pm \frac{i^{\epsilon/2} x^{K+1+\epsilon/2}}{K+1+\epsilon/2}\right). \quad (4.5)$$

(In this formula we give the *controlling factor* of the asymptotic behavior of the wave function; we neglect algebraic contributions.) Note that at the center of the wedges the behavior of the wave function is most strongly

exponential; the centerline of each wedge is an anti-Stokes line. At the edges of the wedges the asymptotic behavior is oscillatory. The lines marking the edges of the wedges are Stokes lines.

For all positive integer values of  $K$  the results are qualitatively similar. At  $\epsilon = 0$  the two wedges are centered about the positive and negative real axes. As  $\epsilon$  increases from 0 the wedges rotate downward and become thinner. In the region  $\epsilon \geq 0$  the eigenvalues are all real and positive and they rise with increasing  $\epsilon$ . As  $\epsilon \rightarrow \infty$ , the two wedges become infinitely thin and lie along the negative imaginary axis. There is no eigenvalue problem in this limit because the solution contour for the Schrödinger equation (4.1) can be pushed off to infinity. Indeed, we find that in this limit the eigenvalues all become infinite.

When  $\epsilon$  is negative, the wedges rotate upward and become thicker. The eigenvalues gradually pair off and become complex starting with the highest eigenvalues. Thus,  $\mathcal{PT}$  symmetry is spontaneously broken for  $\epsilon < 0$ . Eventually, as  $\epsilon$  approaches  $-K$ , only the lowest eigenvalue remains real. At  $\epsilon = -K$  the two wedges join at the positive imaginary axis. Thus, again there is no eigenvalue problem and there are no eigenvalues at all. In the limit  $\epsilon \rightarrow -K$  the one remaining real eigenvalue diverges logarithmically.

The spectrum for the case of arbitrary positive integer  $K$  is quite similar to that for  $K = 1$ . However, in general, when  $K > 1$ , a novel feature emerges: A new transition appears for all negative integer values of  $\epsilon$  between 0 and  $-K$ . At these isolated points the spectrum is entirely real. Just above each of these negative-integer values of  $\epsilon$  the energy levels reemerge in pairs from the complex plane and just below these special values of  $\epsilon$  the energy levels once again pinch off and become complex.

### A. Quantum $x^4(ix)^\epsilon$ theory

The spectrum for the case  $K = 2$  is displayed in Fig. 14. This figure resembles Fig. 11 for the case  $K = 1$ . However, at  $\epsilon = -1$  there is a new transition. This transition is examined in detail in Fig. 15.

An important feature of the spectrum in Fig. 14 is the disappearance of the eigenvalues and divergence of the lowest eigenvalue as  $\epsilon$  decreases to  $-2$ . Following the approach of Sec. III A, we now derive the asymptotic behavior of the ground-state energy as  $\epsilon \rightarrow -2^+$ . To do so we let  $\epsilon = -2 + \delta$  and obtain from Eq. (4.1) the Schrödinger equation

$$-\psi''(x) - x^2(ix)^\delta \psi(x) = E\psi(x). \quad (4.6)$$

We study this differential equation for small positive  $\delta$ .

When  $\delta = 0$  this differential equation (4.6) reduces to

$$-\psi''(x) - x^2\psi(x) = E\psi(x). \quad (4.7)$$

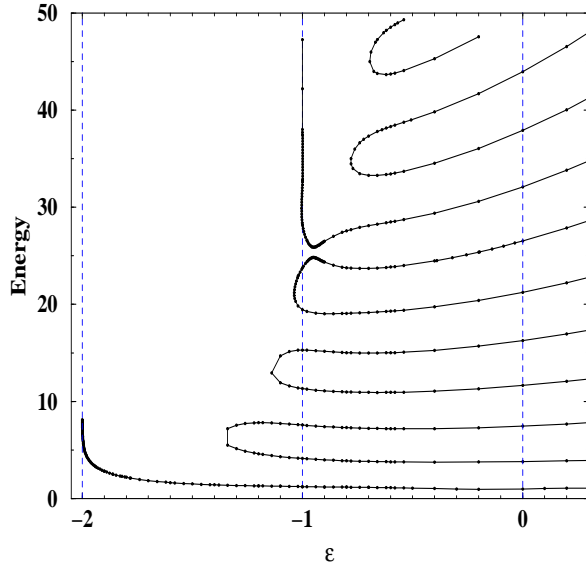


FIG. 14. Energy levels of the Hamiltonian  $H = p^2 + x^4(ix)^\epsilon$  as a function of the parameter  $\epsilon$ . This figure is similar to Fig. 11, but now there are four regions: When  $\epsilon \geq 0$ , the spectrum is real and positive and it rises monotonically with increasing  $\epsilon$ . The lower bound  $\epsilon = 0$  of this  $\mathcal{PT}$ -symmetric region corresponds to the pure quartic anharmonic oscillator, whose Hamiltonian is given by  $H = p^2 + x^4$ . When  $-1 < \epsilon < 0$ ,  $\mathcal{PT}$  symmetry is spontaneously broken. There are a finite number of real positive eigenvalues and an infinite number of complex conjugate pairs of eigenvalues; as a function of  $\epsilon$  the eigenvalues pinch off in pairs and move off into the complex plane. By the time  $\epsilon = -1$  only eight real eigenvalues remain; these eigenvalues are continuous at  $\epsilon = 1$ . Just as  $\epsilon$  approaches  $-1$  the entire spectrum reemerges from the complex plane and becomes real. (Note that at  $\epsilon = -1$  the entire spectrum agrees with the entire spectrum in Fig. 11 at  $\epsilon = 1$ .) This reemergence is difficult to see in this figure but is much clearer in Fig. 15 in which the vicinity of  $\epsilon = -1$  is blown up. Just below  $\epsilon = -1$ , the eigenvalues once again begin to pinch off and disappear in pairs into the complex plane. However, this pairing is different from the pairing in the region  $-1 < \epsilon < 0$ . Above  $\epsilon = -1$  the lower member of a pinching pair is even and the upper member is odd (that is,  $E_8$  and  $E_9$  combine,  $E_{10}$  and  $E_{11}$  combine, and so on); below  $\epsilon = -1$  this pattern reverses (that is,  $E_7$  combines with  $E_8$ ,  $E_9$  combines with  $E_{10}$ , and so on). As  $\epsilon$  decreases from  $-1$  to  $-2$ , the number of real eigenvalues continues to decrease until the only real eigenvalue is the ground-state energy. Then, as  $\epsilon$  approaches  $-2^+$ , the ground-state energy diverges logarithmically. For  $\epsilon \leq -2$  there are no real eigenvalues.

The anti-Stokes lines for this equation lie at  $45^\circ$  and at  $-225^\circ$ . Thus, we rotate the integration contour from the real axis to the anti-Stokes lines and substitute

$$x = \begin{cases} \frac{s}{\sqrt{2}} e^{-\frac{5i\pi}{4}} & (\text{Re } x < 0) \\ \frac{r}{\sqrt{2}} e^{\frac{i\pi}{4}} & (\text{Re } x > 0) \end{cases} \quad (4.8)$$

for  $x$  in the left-half and in the right-half complex plane, respectively. Note as  $s$  and  $r$  increase,  $x$  moves towards

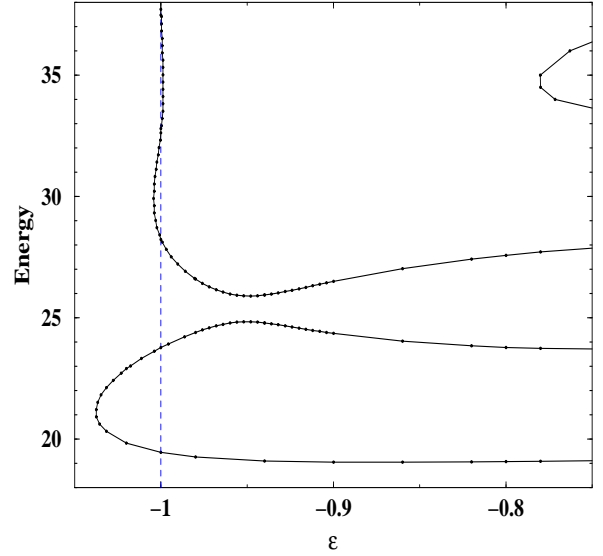


FIG. 15. A magnification of Fig. 14 in the vicinity of the transition at  $\epsilon = -1$ . Just above  $\epsilon = -1$  the entire spectrum reemerges from the complex plane, and just below  $\epsilon = -1$  it continues to disappear into the complex plane. The spectrum is entirely real at  $\epsilon = -1$ .

complex infinity in both the left- and right-half plane.

The wave function in the left-half plane,  $\psi_L(s)$ , and the wave function in the right-half plane,  $\psi_R(r)$ , satisfy the differential equations

$$\begin{aligned} -\frac{d^2}{ds^2}\psi_L(s) + \left(\frac{s^2}{4} - \frac{1}{2}\right)\psi_L(s) &= \nu\psi_L(s), \\ -\frac{d^2}{dr^2}\psi_R(r) + \left(\frac{r^2}{4} - \frac{1}{2}\right)\psi_R(r) &= (-\nu - 1)\psi_R(r), \end{aligned} \quad (4.9)$$

where we have set  $\nu = -\frac{i}{2}E - \frac{1}{2}$ . For each of these equations the solution that vanishes at infinity is a parabolic cylinder function [16]:

$$\begin{aligned} \psi_L(s) &= C_L D_\nu(s) = C_L D_\nu\left(x\sqrt{2}e^{\frac{5i\pi}{4}}\right), \\ \psi_R(r) &= C_R D_{-\nu-1}(r) = C_R D_{-\nu-1}\left(x\sqrt{2}e^{-\frac{i\pi}{4}}\right), \end{aligned} \quad (4.10)$$

where  $C_L$  and  $C_R$  are arbitrary constants.

We impose the quantization condition by patching these solutions together at  $x = 0$  on the real- $x$  axis according to the patching conditions

$$\begin{aligned} \psi_L(x) \Big|_{x=0} &= \psi_R(x) \Big|_{x=0}, \\ \frac{d}{dx}\psi_L(x) \Big|_{x=0} &= \frac{d}{dx}\psi_R(x) \Big|_{x=0}. \end{aligned} \quad (4.11)$$

To eliminate the constants  $C_L$  and  $C_R$  we take the ratio of these two equations and simplify the result by cross multiplying:

$$\left[ \psi_R(x) \frac{d}{dx}\psi_L(x) - \psi_L(x) \frac{d}{dx}\psi_R(x) \right] \Big|_{x=0} = 0. \quad (4.12)$$

We now show that this condition cannot be satisfied by the  $\delta = 0$  wave function in Eq. (4.10). For this case, the quantization condition (4.12) states that

$$D_\nu(s) \frac{d}{ds} D_{-\nu-1}(is) - D_{-\nu-1}(is) \frac{d}{ds} D_\nu(s) \quad (4.13)$$

vanishes at  $s = 0$ . (We have simplified the argument by setting  $s = x\sqrt{2}e^{5i\pi/4}$ .) But Eq. (4.13) for any value of  $s$  is just the Wronskian for parabolic cylinder functions [16] and this Wronskian equals  $-ie^{-i\nu\pi/2}$ . This is a *nonzero* result. Thus, when  $\delta = 0$ , there cannot be any eigenvalue  $E$ , real or complex, and the spectrum is empty.

The quantization condition (4.12) can be satisfied when  $\delta > 0$ . We investigate this region for the case when  $\delta$  is small and positive by performing an asymptotic analysis. We assume that  $E \rightarrow \infty$  as  $\delta \rightarrow 0+$ , but slower than any power of  $\delta$ , and that the wave function  $\psi(x)$  has a formal power series expansion in  $\delta$ :

$$\psi(x) \sim y_0(x) + \delta y_1(x) + O(\delta^2) \quad (\delta \rightarrow 0+). \quad (4.14)$$

Next, we expand the Schrödinger equation (4.6) in powers of  $\delta$ :

$$\begin{aligned} y_0''(x) + x^2 y_0(x) + E y_0(x) &= 0, \\ y_1''(x) + x^2 y_1(x) + E y_1(x) &= -x^2 \ln(ix) y_0(x), \end{aligned} \quad (4.15)$$

and so on.

Of course, to zeroth order in  $\delta$  we obtain Eq. (4.7) for  $y_0(x)$ . Thus, in the left- and right-half complex  $x$ -plane we get

$$\begin{aligned} y_0^L(x) &= C_L D_\nu \left( x\sqrt{2}e^{\frac{5i\pi}{4}} \right), \\ y_0^R(x) &= C_R D_{-\nu-1} \left( x\sqrt{2}e^{-\frac{i\pi}{4}} \right). \end{aligned} \quad (4.16)$$

To first order in  $\delta$ , we simplify the differential equation for  $y_1(x)$  in (4.15) by substituting

$$y_1(x) = Q(x) y_0(x). \quad (4.17)$$

Using the differential equation for  $y_0(x)$  in (4.15), we get

$$y_0(x) Q''(x) + 2y_0'(x) Q'(x) = -x^2 \ln(ix) y_0(x). \quad (4.18)$$

Multiplying this equation by the integrating factor  $y_0(x)$ , we obtain

$$\left[ y_0^2(x) Q'(x) \right]' = -x^2 \ln(ix) y_0^2(x). \quad (4.19)$$

The integral of this equation gives

$$\begin{aligned} Q_L'(x) &= \int_x^{\infty e^{-5i\pi/4}} dt t^2 \ln(it) \left[ \frac{y_0^L(t)}{y_0^L(x)} \right]^2, \\ Q_R'(x) &= \int_x^{\infty e^{i\pi/4}} dt t^2 \ln(it) \left[ \frac{y_0^R(t)}{y_0^R(x)} \right]^2, \end{aligned} \quad (4.20)$$

where the limit of the integral at infinity ensures that  $Q'(x)$  is bounded for  $|x| \rightarrow \infty$ .

To determine the asymptotic behavior of the ground-state eigenvalue as  $\delta \rightarrow 0+$ , we insert

$$\begin{aligned} \psi_{L,R}(x) &\sim y_0^{L,R}(x) + \delta y_1^{L,R}(x) + O(\delta^2) \\ &= y_0^{L,R}(x) [1 + \delta Q^{L,R}(x)] \end{aligned} \quad (4.21)$$

into the quantization condition (4.12):

$$\begin{aligned} 0 &= \left[ \psi_R(x) \frac{d}{dx} \psi_L(x) - \psi_L(x) \frac{d}{dx} \psi_R(x) \right] \Big|_{x=0} \\ &= \left[ y_0^R(x) \frac{d}{dx} y_0^L(x) - y_0^L(x) \frac{d}{dx} y_0^R(x) \right] \Big|_{x=0} \\ &\quad \times [1 + \delta (Q_R(0) + Q_L(0))] \\ &\quad + \delta y_0^R(0) y_0^L(0) [Q_L'(0) - Q_R'(0)]. \end{aligned} \quad (4.22)$$

We are free to choose  $Q_R(0) + Q_L(0) = 0$  to simplify this result.

Substituting the Wronskian for the parabolic cylinder function and the result for  $y_0(0)$  in Eq. (4.16), we obtain

$$\sqrt{2}e^{-\frac{\pi E}{4}} \sim \delta D_\nu(0) D_{-\nu-1}(0) [Q_R'(0) - Q_L'(0)]. \quad (4.23)$$

We can simplify this result using the identity

$$D_\nu(0) = \frac{\sqrt{\pi} 2^{\frac{\nu}{2}}}{\Gamma\left(\frac{1}{2} - \frac{\nu}{2}\right)} \quad (4.24)$$

and  $\nu = -\frac{i}{2}E - \frac{1}{2}$  to obtain

$$D_\nu(0) D_{-\nu-1}(0) = \frac{\Gamma\left(\frac{1}{2} + \frac{\nu}{2}\right) \cos\left(\frac{\pi\nu}{2}\right)}{\Gamma\left(1 + \frac{\nu}{2}\right) \sqrt{2}} \sim \frac{e^{\frac{\pi}{4}E}}{\sqrt{E}}, \quad (4.25)$$

where we have used the reflection formula,  $\Gamma(z)\Gamma(1-z) = \pi/\sin(\pi z)$ , and the asymptotic behavior  $\Gamma(x+1/2)/\Gamma(x+1) \sim x^{-1/2}$  for large  $x$ . Thus, Eq. (4.23) reduces to

$$\frac{\sqrt{2E}}{\delta} e^{-\frac{\pi E}{2}} \sim Q_R'(0) - Q_L'(0). \quad (4.26)$$

We can further show that

$$\begin{aligned} &Q_R'(0) - Q_L'(0) \\ &= \int_0^{\infty e^{i\pi/4}} dt t^2 \ln(it) \left[ \frac{D_{-\nu-1}(\sqrt{2}te^{-i\pi/4})}{D_{-\nu-1}(0)} \right]^2 \\ &\quad - \int_0^{\infty e^{-5i\pi/4}} dt t^2 \ln(it) \left[ \frac{D_\nu(\sqrt{2}te^{5i\pi/4})}{D_\nu(0)} \right]^2 \\ &= - \int_0^{\infty} \frac{t^2 dt}{2^{\frac{3}{2}}} e^{-\frac{i\pi}{4}} \ln\left(\frac{s}{\sqrt{2}} e^{\frac{3i\pi}{4}}\right) \left[ \frac{D_{-\nu-1}(t)}{D_{-\nu-1}(0)} \right]^2 \\ &\quad - \int_0^{\infty} \frac{t^2 dt}{2^{\frac{3}{2}}} e^{\frac{i\pi}{4}} \ln\left(\frac{s}{\sqrt{2}} e^{-\frac{3i\pi}{4}}\right) \left[ \frac{D_\nu(t)}{D_\nu(0)} \right]^2. \end{aligned} \quad (4.27)$$

We observe that the previous expression is real because  $\nu^* = -\nu - 1$  implies that  $D_\nu(t)^* = D_{-\nu-1}(t)$  and thus the two integrals are complex conjugates. Thus, Eq. (4.27) is real, and  $E$  is a real function of  $\delta$ . Furthermore, because the ratio  $D_\nu(t)/D_\nu(0)$  appears in both integrals, the expression can at most vary as a power of  $E$ . Hence, the contribution of  $Q'_R(0) - Q'_L(0)$  to the balance in Eq. (4.26) is subdominant and can be neglected. Our final result for the small- $\delta$  behavior of the lowest eigenvalue is that

$$E \sim -\frac{2}{\pi} \ln \delta + O[\ln(\ln \delta)] \quad (\delta \rightarrow 0^+). \quad (4.28)$$

In Fig. 16 we show that Eq. (4.28) compares well with the numerical data for the lowest eigenvalue in the limit as  $\delta \rightarrow 0$ .

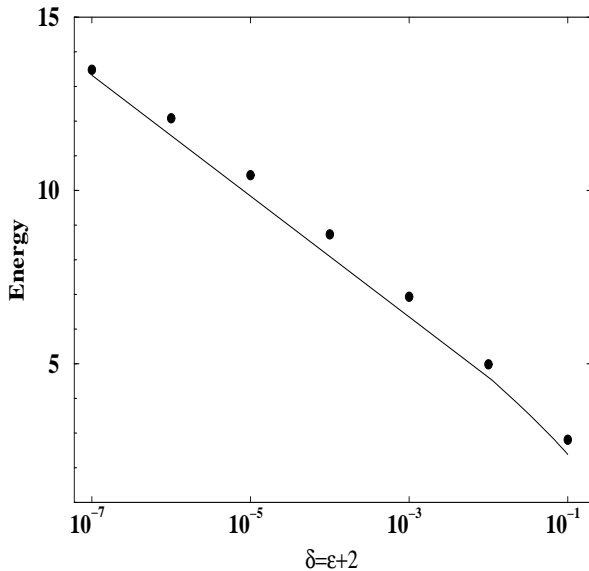


FIG. 16. A comparison of the lowest eigenvalue of the Hamiltonian  $H = p^2 + x^4(ix)^\epsilon$  (solid circles) with the asymptotic prediction in (4.28) (solid line) near  $\epsilon = -2$ . The solid line includes a one parameter fit of terms that grow like  $\ln(\ln \delta)$  as  $\delta \rightarrow 0^+$ .

### B. Classical $x^4(ix)^\epsilon$ theory

It is instructive to compare the quantum mechanical and classical mechanical theories for the case  $K = 2$ . Our objective in doing so is to understand more deeply the breaking of  $\mathcal{PT}$  symmetry that occurs at  $\epsilon = 0$ . For the case  $K = 1$  we found that  $\mathcal{PT}$  symmetry is broken at the classical level in a rather obvious way: Left-right symmetric classical trajectories become spirals as  $\epsilon$  becomes negative (see Fig. 9). However, we find that when  $K = 2$  spirals do not occur until  $\epsilon < -2$ . The classical manifestation of  $\mathcal{PT}$  symmetry breaking for  $-2 \leq \epsilon < 0$  and the transition that occurs at  $\epsilon = 0$  is actually quite subtle.

For purposes of comparison we begin by examining the classical trajectories for the positive value  $\epsilon = 0.7$ . In

Fig. 17 we plot three classical trajectories in the complex- $x$  plane. The first is an arc that joins the classical turning points in the lower-half plane. The other two are closed orbits that surround this arc. The smaller closed orbit remains on the principal sheet and has a period ( $T \approx 4.9$ ), which is equal to that of the arc. The more complicated trajectory is left-right symmetric but extends to three sheets of the Riemann surface. The period ( $T \approx 26.1$ ) of this third orbit is significantly different from and larger than the period of the other two.

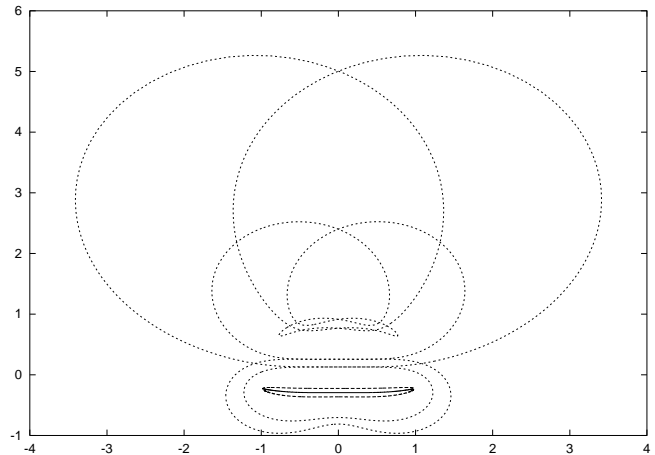


FIG. 17. Three classical trajectories in the complex- $x$  plane for a particle described by the Hamiltonian  $H = p^2 + x^4(ix)^\epsilon$  with  $\epsilon = 0.7$ . The solid line represents oscillatory motion between the classical turning points. The long-dashed line is a nearby trajectory that encloses and has the same period as the solid-line trajectory. The short dashed line has a different topology (it enters three sheets of the Riemann surface) from the long-dashed line, even though these trajectories are very near one another in the vicinity of the turning points. The period of this motion is much longer than that of the solid and long-dashed trajectories.

Next, we consider the negative value  $\epsilon = -0.7$ . In Fig. 18 we plot two classical trajectories for this value. The first (solid line) is an arc joining the classical turning points in the upper-half plane. This arc extends to three sheets of the Riemann surface. The other trajectory (dashed line) is a closed orbit that surrounds this arc. Both have the period  $T \approx 22.3$ . This figure illustrates the first of two important changes that occur as  $\epsilon$  goes below zero. The trajectory that joins the two turning points no longer lies on the principal sheet of the Riemann surface; it exhibits a multisheeted structure.

Figure 19 illustrates the second important change that occurs as  $\epsilon$  goes below zero. On this figure we again plot two classical trajectories for the negative value  $\epsilon = -0.7$ . The first (solid line) is the arc joining the classical turning points in the upper-half plane. This arc is also shown on Fig. 18. The second trajectory (dashed line) is a closed orbit that passes near the turning points. The two trajectories do not cross; the apparent points of intersection are



on different sheets of the Riemann surface. The period of the dashed trajectory is  $T \approx 13.7$ , which is considerably *smaller* than that of the solid line. Indeed, on the basis of extensive numerical studies, it appears that all trajectories for  $-2 < \epsilon < 0$ , while they are  $\mathcal{PT}$  (left-right) symmetric, have periods that are less than or equal to that of the solid line. When  $\epsilon > 0$ , the periods of trajectories increase as the trajectories move away from the oscillatory trajectory connecting the turning points.

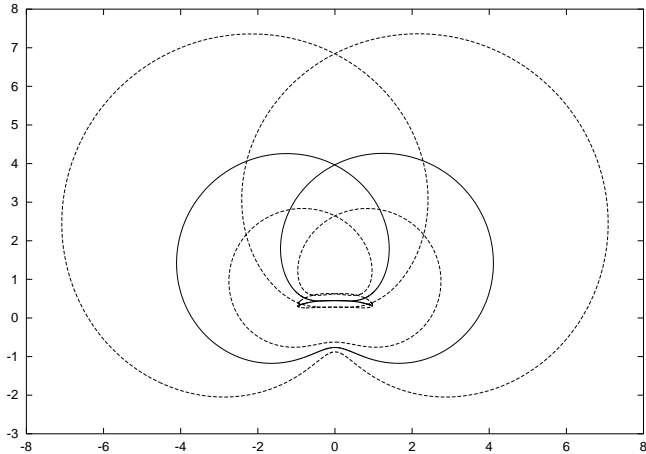


FIG. 18. Two classical trajectories in the complex- $x$  plane for a particle described by the Hamiltonian  $H = p^2 + x^4(ix)^\epsilon$  with  $\epsilon = -0.7$ . The solid line represents oscillatory motion between the classical turning points. This trajectory enters three sheets of the Riemann surface. The dashed line is a nearby trajectory that encloses and has the same period as the solid-line trajectory.

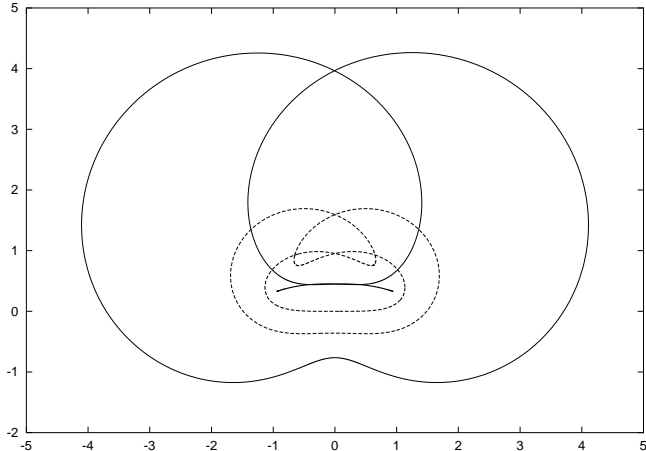


FIG. 19. Two classical trajectories in the complex- $x$  plane for a particle described by the Hamiltonian  $H = p^2 + x^4(ix)^\epsilon$  with  $\epsilon = -0.7$ . The solid line represents oscillatory motion between the classical turning points and is the same as that in Fig. 18. The dashed line is a nearby trajectory whose period is smaller than the period of the solid-line trajectory.

We speculate that for negative values of  $\epsilon$  the appearance of complex eigenvalues in the quantum theory (see

Fig. 14) is associated with an instability. The path integral for a quantum theory is ordinarily dominated by paths in the vicinity of the classical trajectory connecting the turning points. However, when  $\epsilon$  is negative, we believe that these trajectories no longer dominate the path integral because there are more remote trajectories whose classical periods are *smaller*. Thus, the action is no longer dominated by a stationary point in the form of a classical path having  $\mathcal{PT}$  symmetry. Hence, the spectrum can contain complex eigenvalues.

The appearance of a purely real spectrum for the special value  $\epsilon = -1$  is consistent with this conjecture. For integer values of  $\epsilon > -2$  we find that all classical trajectories lie on the principal sheet of the Riemann surface and have the *same* period.

### C. Quantum $x^6(ix)^\epsilon$ theory

The spectrum for the case  $K = 3$  is displayed in Fig. 20. This figure resembles Fig. 14 for the case  $K = 2$ . However, now there are transitions at both  $\epsilon = -1$  and  $\epsilon = -2$ .

## V. COMPLEX DEFORMATIONS OF NONANALYTIC POTENTIALS

In our discussion so far we have considered complex deformations of the potentials  $x^{2K}$ . These potentials are analytic functions of  $x$ . In this section we consider complex deformations of the *nonanalytic* potentials  $|x|^P$ , where  $P$  is real. We will see that the eigenvalues of the potential  $|x|^P(ix)^\epsilon$  are real only when  $\epsilon = 0$  (and sometimes at other isolated values of  $\epsilon$ ). Thus, it appears that if one attempts to construct a complex deformation of a nonanalytic potential, one destroys a crucial property of the theory; namely, that the spectrum be real.

We begin our discussion by examining the spectrum of the  $|x|^P$  potential. The eigenvalues of this potential are displayed as a function of  $P$  in Fig. 21. It is interesting that the spectrum of this potential [17] is quite similar to that of the  $x^2(ix)^\epsilon$  potential for positive  $\epsilon$  (see Fig. 11). The difference between the spectra of these two potentials becomes apparent when  $\epsilon$  is large: As  $\epsilon \rightarrow \infty$ , the spectrum of  $|x|^{2+\epsilon}$  approaches that of the square-well potential [ $E_n = (n+1)^2\pi^2/4$ ], while the energies of the  $x^2(ix)^\epsilon$  potential diverge.

WKB theory gives an excellent approximation to the spectrum of both potentials and thus provides an interesting comparison. For the  $x^2(ix)^\epsilon$  potential, when  $\epsilon \geq 0$ , the novelty of the WKB calculation is that it must be performed in the complex plane. The turning points  $x_\pm$  are those roots of  $E - x^2(ix)^\epsilon = 0$  that *analytically continue* off the real axis as  $\epsilon$  moves away from zero (the harmonic oscillator):

$$x_- = E^{\frac{1}{2+\epsilon}} e^{i\pi \frac{4+3\epsilon}{4+2\epsilon}}, \quad x_+ = E^{\frac{1}{2+\epsilon}} e^{-\frac{i\pi\epsilon}{4+2\epsilon}}. \quad (5.1)$$

These turning points lie in the lower-half (upper-half)  $x$  plane when  $\epsilon > 0$  ( $\epsilon < 0$ ).

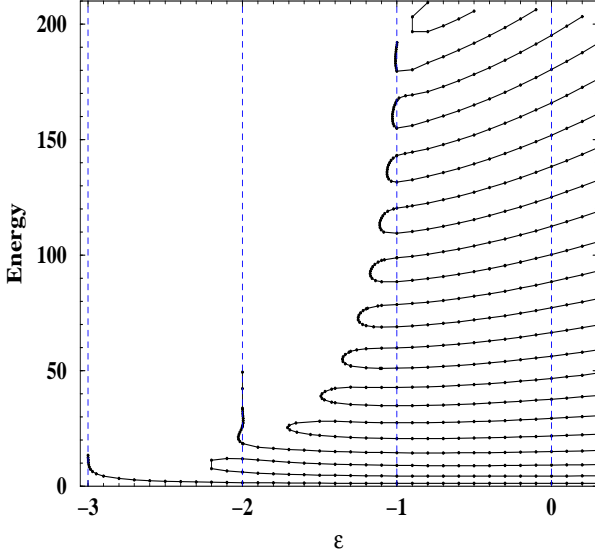


FIG. 20. Energy levels of the Hamiltonian  $H = p^2 + x^6(ix)^\epsilon$  as a function of the parameter  $\epsilon$ . This figure is similar to Fig. 14, but now there are five regions: When  $\epsilon \geq 0$ , the spectrum is real and positive and it rises monotonically with increasing  $\epsilon$ . The lower bound  $\epsilon = 0$  of this  $\mathcal{PT}$ -symmetric region corresponds to the pure sextic anharmonic oscillator, whose Hamiltonian is given by  $H = p^2 + x^6$ . The other four regions are  $-1 < \epsilon < 0$ ,  $-2 < \epsilon < -1$ ,  $-3 < \epsilon < -2$ , and  $\epsilon < -3$ . The  $\mathcal{PT}$  symmetry is spontaneously broken when  $\epsilon$  is negative, and the number of real eigenvalues decreases as  $\epsilon$  becomes more negative. However, at the boundaries  $\epsilon = -1$ ,  $-2$  there is a complete real positive spectrum. When  $\epsilon = -1$ , the eigenspectrum is identical to the eigenspectrum in Fig. 14 at  $\epsilon = 1$ . For  $\epsilon \leq -3$  there are no real eigenvalues.

The leading-order WKB phase-integral quantization condition is

$$\frac{2n+1}{2}\pi = \int_{x_-}^{x_+} dx \sqrt{E - x^2(ix)^\epsilon}. \quad (5.2)$$

It is crucial that this integral follow a path along which the *integral is real*. When  $\epsilon > 0$ , this path lies entirely in the lower-half  $x$  plane and when  $\epsilon = 0$  the path lies on the real axis. But, when  $\epsilon < 0$  the path is in the upper-half  $x$  plane; it crosses the cut on the positive-imaginary axis and thus is *not a continuous path joining the turning points*. Hence, WKB fails when  $\epsilon < 0$ .

When  $\epsilon \geq 0$ , we deform the phase-integral contour so that it follows the rays from  $x_-$  to 0 and from 0 to  $x_+$ :

$$\frac{2n+1}{2}\pi = 2 \sin\left(\frac{\pi}{2+\epsilon}\right) E^{\frac{4+\epsilon}{4+2\epsilon}} \int_0^1 ds \sqrt{1-s^{2+\epsilon}}. \quad (5.3)$$

We then solve for  $E_n$ :

$$E_n \sim \left[ \frac{\Gamma\left(\frac{8+3\epsilon}{4+2\epsilon}\right) \sqrt{\pi}(n+1/2)}{\sin\left(\frac{\pi}{2+\epsilon}\right) \Gamma\left(\frac{3+\epsilon}{2+\epsilon}\right)} \right]^{\frac{4+2\epsilon}{4+\epsilon}} \quad (n \rightarrow \infty). \quad (5.4)$$

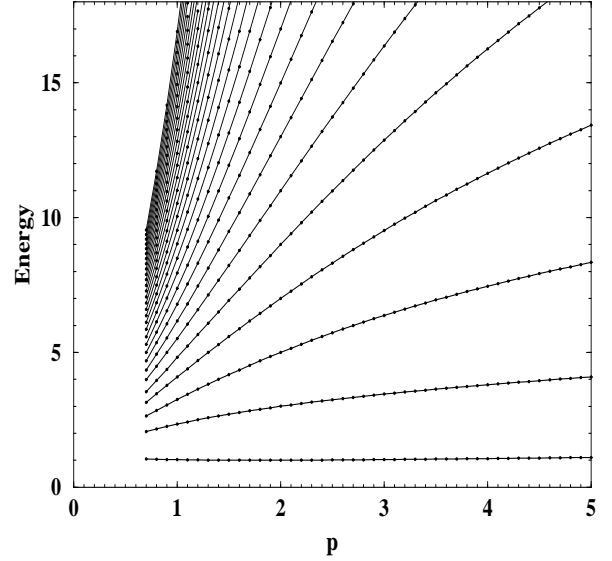


FIG. 21. Energy levels of the Hamiltonian  $H = p^2 + |x|^P$  as a function of the parameter  $P$ . This figure is similar to Fig. 11, but the eigenvalues do not pinch off and go into the complex plane because the Hamiltonian is Hermitian (spectrum becomes dense at  $P = 0$ ).

We can perform a higher-order WKB calculation by replacing the phase integral by a *closed contour* that encircles the path connecting the two turning points (see Ref. [18]). With  $Q(x) = x^2(ix)^\epsilon - E$ , the next to leading-order WKB quantization condition is

$$\frac{2n+1}{2}\pi = \frac{1}{2i} \oint_C dx \sqrt{Q(x)} + \frac{1}{2i} \oint_C dx \frac{Q''(x)}{48Q(x)^{\frac{3}{2}}}, \quad (5.5)$$

where the contour  $C$  encircles the turning points  $x_+$  and  $x_-$  in a counterclockwise direction. As above, we deform the contour to lie above and below the rays that connect the turning points with  $x = 0$ , we obtain for the second contour integral in Eq. (5.5):

$$\begin{aligned} & \frac{1}{2i} \oint_C dx \frac{Q''(x)}{48Q(x)^{\frac{3}{2}}} \\ &= -E^{-\frac{4+\epsilon}{4+2\epsilon}} \frac{2+3\epsilon+\epsilon^2}{12} \sin\left(\frac{\pi}{2+\epsilon}\right) \int_0^1 ds \frac{s^\epsilon}{(1-s^{2+\epsilon})^{\frac{3}{2}}} \\ &= -E^{-\frac{4+\epsilon}{4+2\epsilon}} \frac{\epsilon}{24} \sin\left(\frac{\pi}{2+\epsilon}\right) \frac{\Gamma\left(\frac{3+2\epsilon}{2+\epsilon}\right)}{\Gamma\left(\frac{5+3\epsilon}{4+2\epsilon}\right)}. \end{aligned} \quad (5.6)$$

We add the contribution of this integral to the leading-order result in Eq. (5.3) and solve the resulting expression for the energy  $E$ , assuming that  $n$  is large, and obtain

$$E_n \sim \left[ \frac{\Gamma\left(\frac{8+3\epsilon}{4+2\epsilon}\right) \sqrt{\pi}(n+1/2)}{\sin\left(\frac{\pi}{2+\epsilon}\right) \Gamma\left(\frac{3+\epsilon}{2+\epsilon}\right)} \right]^{\frac{4+2\epsilon}{4+\epsilon}} \times \left[ 1 + \frac{(2+\epsilon)(1+\epsilon) \sin\left(\frac{2\pi}{2+\epsilon}\right)}{6\pi\left(n+\frac{1}{2}\right)^2(4+\epsilon)^2} \right] \quad (n \rightarrow \infty). \quad (5.7)$$

This is the next-to-leading-order WKB result for the energy.

The next correction to the WKB result for the  $|x|^{2+\epsilon}$  potential is

$$E_n \sim \left[ \frac{\Gamma\left(\frac{8+3\epsilon}{4+2\epsilon}\right) \sqrt{\pi}(n+1/2)}{\Gamma\left(\frac{3+\epsilon}{2+\epsilon}\right)} \right]^{\frac{4+2\epsilon}{4+\epsilon}} \times \left[ 1 + \frac{(2+\epsilon)(1+\epsilon) \cot\left(\frac{\pi}{2+\epsilon}\right)}{3\pi\left(n+\frac{1}{2}\right)^2(4+\epsilon)^2} \right] \quad (n \rightarrow \infty), \quad (5.8)$$

Note that the leading-order WKB quantization condition (accurate for  $\epsilon > -2$ ) for the  $|x|^{2+\epsilon}$  potential is like Eq. (5.4) except that  $\sin\left(\frac{\pi}{2+\epsilon}\right)$  is absent.

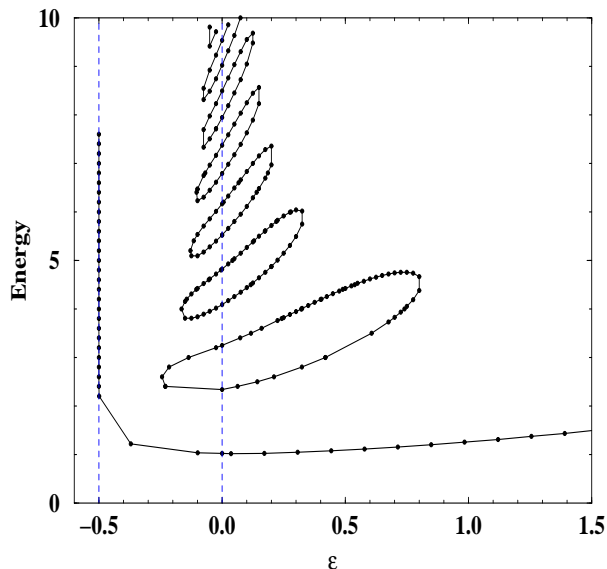


FIG. 22. Energy levels of the Hamiltonian  $H = p^2 + |x|(ix)^\epsilon$  as a function of the parameter  $\epsilon$ . The spectrum is entirely real only when  $\epsilon = 0$ .

Now we examine what happens when we attempt to deform the  $|x|^P$  potential using a complex deformation. That is, we consider an  $|x|^P(ix)^\epsilon$  potential. Of course, since  $|x|$  is not an analytic function, we cannot define an analytic continuation of the Schrödinger eigenvalue problem

$$-\frac{d^2}{dx^2}\psi(x) + |x|^P(ix)^\epsilon\psi(x) = E\psi(x) \quad (5.9)$$

into the complex- $x$  plane; we cannot unambiguously define the rotation of wedges in which the boundary conditions apply. However, for sufficiently small  $\epsilon$  we can allow  $x$  to remain *real* and we can impose the boundary condition that  $\psi(x) \rightarrow 0$  for  $x \rightarrow \pm\infty$ . Specifically, we have the condition for *all*  $P$  that if  $|\epsilon| < 2$ , then this boundary condition on the real- $x$  axis may be consistently imposed to define the eigenspectrum.

We now consider two cases:  $P = 1$  (Fig. 22) and  $P = 3$  (Fig. 23). Figure 22 is quite similar to Fig. 11 and Fig. 23 resembles Fig. 14. The key properties of these figures are that (1) the lowest energy level diverges at  $\epsilon = -P/2$ , and that (2) the energy levels pinch off and go into the complex plane on *both* sides of  $\epsilon = 0$ . Thus, the spectrum is entirely real only when  $\epsilon = 0$ .

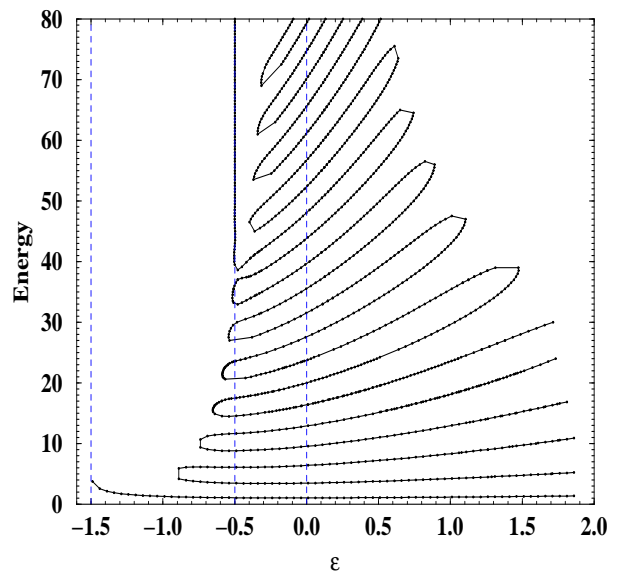


FIG. 23. Energy levels as a function of the parameter  $\epsilon$  for the Hamiltonian  $H = p^2 + |x|^3(ix)^\epsilon$ . The spectrum is real when  $\epsilon = 0$  and  $\epsilon = -0.5$ .

## ACKNOWLEDGEMENT

We thank D. Bessis, M. Flato, J. Wess, A. Wightman, and Y. Zarmi for helpful conversations. We are grateful to the U.S. Department of Energy for financial support.

- 
- [1] C. M. Bender and S. Boettcher, Phys. Rev. Lett. **80**, 5243 (1998). Note that in this reference the notation  $N$  represents the quantity  $2 + \epsilon$ .
  - [2] Several years ago, D. Bessis and J. Zinn-Justin conjectured that the spectrum of  $H$  in Eq. (1.1) for the special case  $\epsilon = 1$  is real (private communication). A partial proof for the reality of the spectrum in this special

- case has been given by M. P. Blencowe, H. Jones, and A. P. Korte, Phys. Rev. D **57**, 5092 (1998) using the linear delta expansion and by E. Delabaere and F. Pham, Ann. Phys. **261**, 180 (1997) using WKB methods.
- [3] T. J. Hollowood, Nucl. Phys. B **386**, 166(1992).
  - [4] D. R. Nelson and N. M. Shnerb, Phys. Rev. E **58**, 1383 (1998).
  - [5] N. Hatano and D. R. Nelson, Phys. Rev. Lett. **77**, 570 (1996), and Phys. Rev. B **56**, 8651 (1997).
  - [6] C. M. Bender and S. Boettcher, J. Phys. A: Math. Gen. **31**, L273 (1998).
  - [7] C. M. Bender and K. A. Milton, Phys. Rev. D **55**, R3255 (1997).
  - [8] Nontriviality of  $-g\phi^4$  field theory has been argued using analytic continuation techniques [see K. Gawadzki and A. Kupiainen, Nucl. Phys. B **257**, 474 (1985)] and using Gaussian approximation [see B. Rosenstein and A. Kovner, Phys. Rev. D **40**, 504 (1989)].
  - [9] C. M. Bender and K. A. Milton, Phys. Rev. D **57**, 3595 (1998).
  - [10] C. M. Bender, S. Boettcher, H. F. Jones, and P. N. Meisinger, in preparation.
  - [11] C. M. Bender and K. A. Milton, submitted.
  - [12] Equation (2.3) is a complex version of the statement that the velocity is the time derivative of the position ( $v = \frac{dx}{dt}$ ). Here, the time is real but the velocity and position are complex.
  - [13] C. M. Bender and J. P. Vinson, J. Math. Phys. **37**, 4103 (1996).
  - [14] M. Abramowitz and I. A. Stegun, *Handbook of Mathematical Functions* (Dover, New York, 1964).
  - [15] C. M. Bender and A. Turbiner, Phys. Lett. A **173**, 442 (1993).
  - [16] A. Erdelyi, W. Magnus, F. Oberhettinger, and F. G. Tricomi, *Higher Transcendental Functions* (McGraw-Hill, New York, 1953), Vol. 2.
  - [17] S. Boettcher and C. M. Bender, J. Math. Phys. **31**, 2579 (1990).
  - [18] C. M. Bender and S. A. Orszag, *Advanced Mathematical Methods for Scientists and Engineers* (McGraw-Hill, New York, 1978), Chap. 10.